



Models for Predicting Biometric Variables in Cowpea Using Multispectral Aerial Images



Brazilian Agricultural Research Corporation
Embrapa Mid-Nort
Ministry of Agriculture, Livestock and Food Supply

**BOLETIM DE PESQUISA
E DESENVOLVIMENTO
154**

**Models for Predicting Biometric Variables in
Cowpea Using Multispectral Aerial Images**

Aderson Soares de Andrade Júnior
Amanda Hellen Sales Sobral
Edson Alves Bastos
Francinaldo Nunes Pessoa Filho
Leandro Pessoa Nunes
Henrique Roig

Embrapa Meio-Norte
Teresina, PI
2023

Embrapa Meio-Norte Local Publication Committee

Av. Duque de Caxias, 5.650,
Bairro Buenos Aires
Caixa Postal 01
64008-480, Teresina, PI, Brazil
www.embrapa.br/meio-norte
www.embrapa.br/fale-conosco/sac

President
Braz Henrique Nunes Rodrigues

Executive secretary
Edna Maria Sousa Lima

Members
Lígia Maria Rolim Bandeira, Orlane da Silva Maia, Maria Eugênia Ribeiro, Kaesel Jackson Damasceno Silva, Ana Lúcia Horta Barreto, José Oscar Lustosa de Oliveira Júnior, Marcos Emanuel da Costa Veloso, Flávio Favaro Blanco, Francisco de Brito Melo, Izabella Cabral Hassum, Tânia Maria Leal, Francisco das Chagas Monteiro, José Alves da Silva Câmara.

Editorial supervision
Lígia Maria Rolim Bandeira

Text revision
Francisco de Assis David da Silva

Bibliographic standardization
Orlane da Silva Maia

Electronic publishing
Jorimá Marques Ferreira

Cover photo
Aderson Soares de Andrade Júnior

1st edition
Digital publishing - PDF (2023)

All rights reserved.

Unauthorized reproduction of this publication, in part or in whole, constitutes breach of copyright (Law 9,610).

Cataloging-in-Publication (CIP) Data
Embrapa Mid-Nort

Models for predicting biometric variables in cowpea using multispectral aerial images / Aderson Soares de Andrade Júnior ... [et al.]. – Teresina : Embrapa Meio-Norte, 2023.
PDF (54 p.) : il. ; 16 cm x 22 cm. – (Boletim de Pesquisa e Desenvolvimento / Embrapa Meio-Norte, 154).

1. Precision agriculture. 2. Remote sensing. 3. Spatial variability. 4. RPA.
5. QGIS. I. Série.

Sumário

Abstract	5
Resumo	7
Introduction.....	8
Material and Methods.....	9
Results and Discussion.....	18
Conclusion.....	49
References	49

Models for Predicting Biometric Variables in Cowpea Using Multispectral Aerial Images

Aderson Soares de Andrade Júnior¹

Amanda Hellen Sales Sobral²

Edson Alves Bastos¹

Francinaldo Nunes Pessoa Filho³

Leandro Pessoa Nunes³

Henrique Roig⁴

Abstract – Models based on vegetation indices (VI) from digital aerial images are promising for predicting biometric variables in agricultural crops. The objective of this study was to generate prediction models for leaf area index (LAI) and shoot dry weight (SDW) of cowpea crops (cultivar BRS-Inhuma) based on VI derived from aerial images captured by a multispectral camera attached to a drone. The study was conducted at the experimental station of the Brazilian Agricultural Research Corporation (Embrapa Mid-North), in Teresina, PI, Brazil (5°05'S, 42°29'W, and altitude of 72 m) from September to October 2022. LAI was measured in the field and in laboratory, while SDW was measured in eight samples at 13, 19, 26, 33, 40, 47, 51, and 61 days after sowing. During this same period, aerial images were captured by a multispectral camera, with four bands (Green, Red, Near-Infrared, and Red-Edge). Fifteen VIs were evaluated through the indicators Pearson correlation and linear regression analyses, and maps were developed to assess spatial variability in the field. The coefficient of determination (R^2), root mean square error (RMSE), and normalized RMSE (nRMSE) were used to validate the models. Models based on cumulative VI during the crop cycle were promising for predicting LAI and SDW (leaves and total) of cowpea plants. Quadratic polynomial models using

¹Researcher, Embrapa Mid-North, Teresina, PI, Brazil.

²Master's Student, Graduate Program in Agronomy, Federal University of Piauí (UFPI), Teresina, PI, Brazil.

³Undergraduate Student, Agronomy Program, State University of Piauí (UESPI), Teresina, PI, Brazil.

⁴Professor, Institute of Geosciences, University of Brasília (UnB), Brasília, DF, Brazil.

the cumulative VIs GCI [$R^2 = 0.8244$ ($p < 0.01$), RMSE = 1.14, and nRMSE = 16.5%] and SR [$R^2 = 0.8358$ ($p < 0.01$), RMSE = 1.18, and nRMSE = 17.1%] enabled LAI prediction, considering the LAI measured in the field with a ceptometer. Linear models using the cumulative VIs TCARI-RE [$R^2 = 0.93$ ($p < 0.001$), RMSE = 22.7 g m⁻², and nRMSE = 10.2%] and TCARI [$R^2 = 0.9176$ ($p < 0.001$), RMSE = 24.8 g m⁻², and nRMSE = 11.1%] are promising for predicting leaf dry weight, whereas the cumulative VIs SR [$R^2 = 0.9693$ ($p < 0.001$), RMSE = 62.5 g m⁻², and nRMSE = 7.0 %] and GCI [$R^2 = 0.9669$ ($p < 0.001$), RMSE = 65.9 g m⁻², and nRMSE = 7.4 %] are promising for predicting cowpea total dry weight. The quality of the models enabled the detection of spatial variability of LAI and SDW in cowpea plants across the entire experimental area.

Keywords: precision agriculture, remote sensing, RPA, QGIS, spatial variability

Modelos de Predição de Variáveis Biométricas em Feijão-Caupi por Imagens Aéreas Multiespectrais

Resumo – Modelos baseados em índices de vegetação (IVs) oriundos de imagens aéreas digitais são promissores na predição de variáveis biométricas das culturas agrícolas. O objetivo do estudo foi a geração de modelos de predição da área foliar e biomassa seca da parte aérea em feijão-caupi, cv BRS Inhuma, baseados em IVs oriundos de imagens aéreas obtidas por câmera multiespectral embarcada em drone. O estudo foi conduzido na estação experimental da Embrapa Meio-Norte, em Teresina, PI, Brasil (5°05' S, 42°29' W e 72 m de altitude), em setembro a outubro de 2022. Quantificou-se em campo e em laboratório a área foliar (IAF) e a biomassa seca da parte aérea em oito amostragens aos 13, 19, 26, 33, 40, 47, 51 e 61 dias após semeadura. Nas mesmas datas, procedeu-se a aquisição das imagens aéreas com uma câmera multiespectral, com quatro bandas (Green, Red, NIR e Red-Edge). Avaliou-se 15 IVs por meio de indicadores como análise de correlação de Pearson e de regressão linear e a geração de mapas para avaliação da variabilidade espacial em campo. Utilizou-se para validação dos modelos o coeficiente de determinação (R^2), a raiz quadrada do erro quadrado médio (RMSE) e o RMSE normalizado (nRMSE). Os modelos baseados em IVs cumulativos durante o ciclo de cultivo foram promissores na predição do IAF e biomassa seca da parte aérea (folhas e total) do feijão-caupi. Modelos polinomiais quadráticos com os IVs GCI-Ac [$R^2 = 0,8244$ ($p < 0,01$); RMSE = 1,14 e nRMSE = 16,5%] e SR-Ac [$R^2 = 0,8358$ ($p < 0,01$); RMSE = 1,18 e nRMSE = 17,1%] permitem a predição do IAF em relação aos dados de IAF medidos em campo com ceptômetro. Modelos lineares com os IVs TCARI-RE-Ac [$R^2 = 0,93$ ($p < 0,001$); RMSE = 22,7 g m⁻² e nRMSE = 10,2%] e TCARI-Ac [$R^2 = 0,9176$ ($p < 0,001$); RMSE = 24,8 g m⁻² e nRMSE = 11,1%] são promissores para a predição da biomassa seca das folhas, enquanto os IVs SR-Ac [$R^2 = 0,9693$ ($p < 0,001$); RMSE = 62,5 g m⁻² e nRMSE = 7,0 %] e GCI-Ac [$R^2 = 0,9669$ ($p < 0,001$); RMSE = 65,9 g m⁻² e nRMSE = 7,4 %] para

a predição da biomassa seca total do feijão-caupi. A qualidade dos modelos possibilitou detectar a variabilidade espacial do IAF e biomassa seca da parte aérea do feijão-caupi em toda a área experimental.

Palavras-chave: agricultura de precisão, sensoriamento remoto, ARP, QGIS, variabilidade espacial

Introduction

Cowpea (*Vigna unguiculata* L. Walp) is an essential food in the dietary intake and the main source of plant proteins for the population in the Northeast region of Brazil (Freire Filho, 2011). In the 2022/2023 crop season, 1,035,900 ha were grown with cowpea in this region, with a production of 441,200 Mg and a mean grain yield of 426 kg ha⁻¹ (Feijão, 2023). Increasing the crop production potential requires the incorporation of new cultivars tolerant to the main biotic and abiotic factors, as well as the adoption of management practices that maximize production factors. Therefore, cowpea production systems, mainly in large areas, demand the adoption of technologies focused on precision agriculture precepts (Mulla, 2013).

Quantitative evaluations of biometric variables such as plant height, leaf area index, and leaf dry weight, which affect grain yield, are essential for a proper precision agriculture system (Bendig et al., 2015; Andrade Junior et al., 2021). Efficient and non-destructive monitoring of plant growth is essential for managing crops focused on precision agriculture (Quille-Mamani et al., 2022).

Shoot dry weight (SDW) and leaf area index (LAI) can be estimated through spectral reflectance measurements of crop canopies (Han et al., 2019; Gano et al., 2021; Ji et al., 2023). However, these measurements involve the use of high-technology and costly equipment, which commonly require calibration. The use of remote sensing techniques employing aerial images captured by drones is recommended as an alternative due to its several over conventional field-sampling methods (destructive) (Andrade Junior et al., 2021; Ji et al., 2022; Quille-Mamani et al., 2022).

Studies have shown that LAI (Santana et al., 2016; Gano et al., 2021) and SDW (Bendig et al., 2015; Han et al., 2019; Quille-Mamani et al., 2022; Ji et al., 2023) can be estimated using prediction models based on vegetation indices obtained from multispectral aerial images captured by drones, as found for common bean (*Phaseolus vulgaris* L.) and fava bean (*Vicia faba* L.) crops evaluated by Ji et al. (2022), Quille-Mamani et al. (2022) and Ji et al. (2023). The results have shown that vegetation index-based models using digital aerial images are promising for predicting SDW in agricultural crops. However, no studies were found focused on generating prediction models for biometric variables in cowpea, such as LAI and SDW, using aerial images from drones.

In this context, the objective of the present study was to generate prediction models for biometric variables (LAI and SDW) in cowpea based on vegetation indices from aerial images captured by a multispectral camera attached to a drone. The study aligns with Sustainable Development Goal 2 (Zero hunger and sustainable agriculture), notably target 2.4 of the 2030 Agenda of the United Nations (UN), as it proposes the adoption of digital technologies to increase productive efficiency, making production systems for food crops, such as cowpea, more sustainable.

Material and Methods

The study was conducted at the experimental station of the Brazilian Agricultural Research Corporation (Embrapa Mid-North), in Teresina, PI, Brazil (5°05'S, 42°29'W, and altitude of 72 m). Aerial images were obtained in an area of 0.6 ha, where three weighing lysimeters were installed to measure the water demand of cowpea crops (Figure 1). The experimental area had a conventional fixed-sprinkler irrigation system consisting of eight lateral rows with sprinkler spacing of 12×12 m. The climate of the region is C1sA'a', characterized as subhumid dry, megathermic, with moderate water surplus in the summer, according to the climate classification of Thornthwaite and Mather (1955).

Historically, the region presents a mean annual temperature of 28.2 °C, with maximum of 34 °C and minimum of 22.4 °C, a mean relative air humidity of 69.5%, and a mean annual rainfall depth of 1,318 mm (Bastos; Andrade Júnior, 2019).

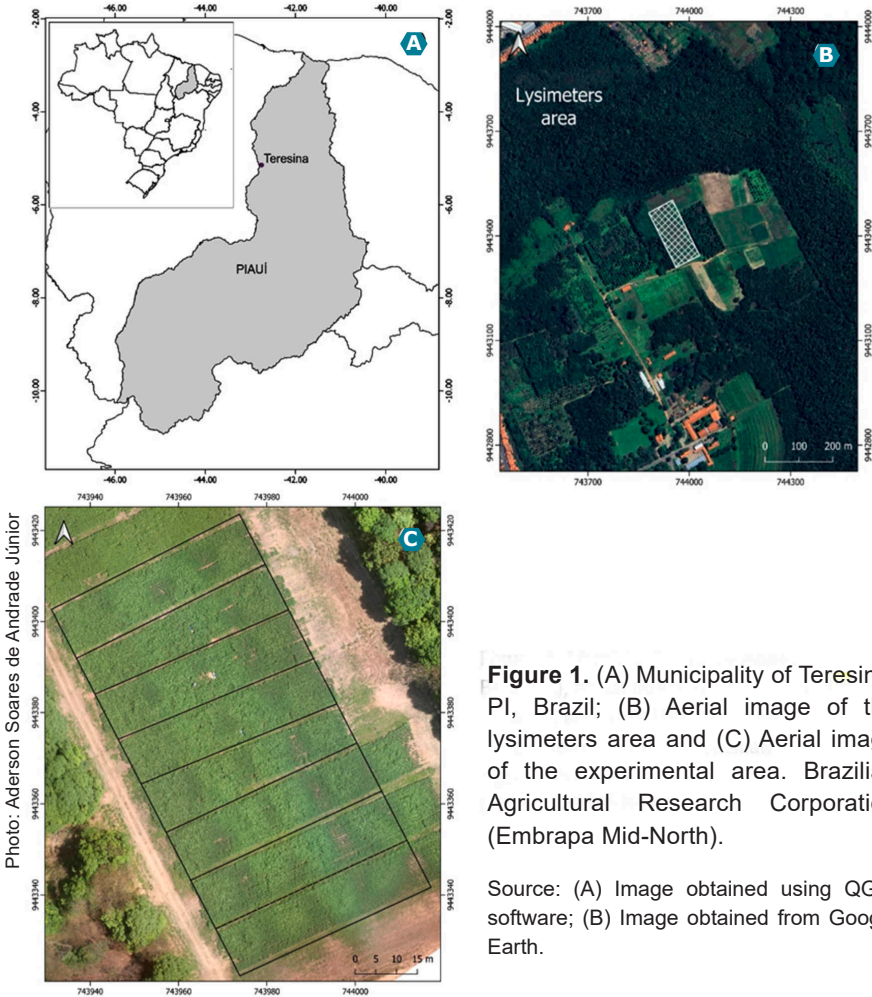


Figure 1. (A) Municipality of Teresina, PI, Brazil; (B) Aerial image of the lysimeters area and (C) Aerial image of the experimental area. Brazilian Agricultural Research Corporation (Embrapa Mid-North).

Source: (A) Image obtained using QGIS software; (B) Image obtained from Google Earth.

Irrigation management was based on the full replacement of reference evapotranspiration (ET_o), estimated daily by the Penman-Monteith method (Allen et al., 1998), considering daily climate data obtained from an automatic weather station located at 500 m from the experimental area. The total irrigation water depth applied was 194.7 mm from sowing (August 31, 2022) to harvest (November 1, 2022), totaling 63 days, with a uniform mean distribution of 74.5%. A total rainfall depth of 25.8 mm was recorded, resulting in a total applied water depth of 220.5 mm (irrigation plus rainfall).

The soil in the experimental area was classified as Typic Hapludult (Argissolo Vermelho-Amarelo distrófico) (Santos et al., 2018; Melo et al., 2019), whose chemical and physical-hydrological characteristics are shown in Table 1. Soil fertilizers were applied according to the soil analysis and recommendations for cowpea crops (Melo et al., 2018).

Table 1. Chemical and physical-hydraulic characterization of the soil in the experimental area processed at the Embrapa Meio-Norte Soil Laboratory. Teresina, PI, 2022.

Layer (m)	OM g kg ⁻¹	pH H ₂ O	P mg dm ⁻³	K Mg Ca Na				CEC	BS %
				cmolc dm ⁻³					
0.0-0.2	12.9	5.78	31.12	0.09	0.35	0.78	0.02	2.94	42.32
0.2-0.4	11.2	5.95	23.49	0.09	0.42	0.73	0.02	2.89	44.11

Layer (m)	Density (g cm ⁻³)	Sand	Silt g kg ⁻¹	Clay	Θcc	
					Θmp	
0.0-0.2	1.63	814.7	94.7	90.7	21.9	
0.2-0.4	1.64	761.9	109.7	128.4	20.8	

OM = organic matter; CEC = cation exchange capacity; BS = base saturation; Θ_{cc} = field capacity; Θ_{mp} = permanent wilting point.

The evaluated cowpea cultivar (BRS-Inhuma) exhibits an indeterminate growth habit, a semi-prostrate architecture, and a medium-early maturation cycle (70-75 days). The seeds were sown using a four-row seed-fertilizer drill, with a spacing of 0.5 m between rows and ten

seeds per meter (20 plants m⁻²). The sowing was carried out on August 31, 2022, and the grains were harvested on November 01, 2022.

Leaf area index (LA) and shoot dry weight (SDW) were measured during the cowpea crop cycle on five randomly selected plant rows, considering all plants within a linear meter. The plants were cut at ground level, placed in plastic bags, and taken to the Plant Physiology Laboratory of Embrapa Mid-North. In the laboratory, the plants were counted and weighed to obtain the total fresh weight of the sample. A subsample equivalent to 1/3 of the plants was taken from this sample, weighed again to obtain the total fresh weight of the subsample, and separated into leaves, stems, flowers, and pods to obtain the total SDW. Total SDW was determined by drying the plants until constant weight in a forced-air circulation oven at 65 °C. The dry weight of the subsample plants was converted to dry weight per unit area (kg m⁻²), using the dry-to-fresh weight ratio of the sample from each replication as a correction factor.

LAI was determined using two different methods: in the laboratory and in the field (non-destructive). In the laboratory, the same plants separated for determining dry weight was used to measure leaf area (LA) using a leaf area meter (LI-3100; Licor, Lincoln, USA). The LA of the plants was used to calculate the leaf area index (LAI) through Equation 1:

$$LAI = (LA \times NP) / AS \dots\dots\dots (1)$$

where: LAI = leaf area index (m² leaves/m² soil); LA = mean leaf area of the subsample plants (m²); NP = number of sampled plants; AS = soil area occupied by the sampled plants (m²).

LAI was measured in the field using a ceptometer (Accupar, LP-80; Decagon Devices, Pullman, USA). The device enabled the obtaining of LAI through by the ratio between the mean photosynthetically active radiation above and below the crop canopy. Measurements were taken at the same locations where the plants were collected for determining

SDW. LAI and SDW measurements were carried out on eight sampling days: at 13, 19, 26, 33, 40, 47, 51, and 61 days after sowing.

Aerial images were acquired using a remotely piloted aircraft, a hexacopter type (Phantom 3 Pro; DJI, Shenzhen, China). Eight flights were conducted on the same days as the plant sampling for LAI and SDW evaluations, between 10:00 a.m. and 11:00 a.m. The flight plan was created in the software Pix4D Capture®. The flight plan was designed to ensure that images were captured with 80% lateral and frontal overlaps, keeping the flight altitude at 40 meters above ground level, with a ground sample distance (GSD) of 2.5 cm pixel⁻¹.

Multispectral images were acquired using a Parrot Sequoia camera (Parrot, Jemmapes, Paris, France) consisted of four sensors that capture images in the spectral bands Green (550 nm), Red (660 nm), Red Edge (735 nm), and Near InfraRed (NIR) (790 nm). The camera resolution is 4608×3456 pixels for each band, and the images are recorded in 16-bit TIFF format.

The images obtained in each flight totaled 186 images per spectral band; they were georeferenced and corrected using a Global Positioning System (GPS) and a solar radiation sensor installed on the top of the aircraft. A radiometric calibration standard was also used for image correction. The processing for generating the orthomosaic of the aerial images was performed in the software Pix4D Mapper® (Pix4D SA, Lausanne, Switzerland). The software configuration enabled the generation of orthomosaic with a spatial resolution of 4.8 cm pixel⁻¹.

Fifteen vegetation indices (VI) were evaluated; they were estimated based on the bands of the multispectral image. Table 2 presents a descriptive summary of the indices used, with basic information regarding their names, abbreviations, equations, and references.

Table 2. Descriptive summary of the multispectral vegetation indices evaluated.

Vegetation indices	Equation	Reference
Green Chlorophyll Index – GCI	$(R_n/R_g) - 1$	Gitelson et al. (2003)
Green Normalized Difference Vegetation Index – gNDVI	$(R_n - R_g)/(R_n + R_g)$	Gitelson e Merzlyak (1998)
Modified Triangular Vegetation Index - MTVI2	$\frac{1,5[1,2(R_n - R_g) - 2,5(R_r - R_g)]}{\sqrt{[(2R_n + 1)^2 - (6R_n - 5\sqrt{R_r}) - 0,5]}}$	Haboudane et al. (2004)
Normalized Difference Red-Edge Index – NDREI	$(R_{RE} - R_g)/(R_{RE} + R_g)$	Hassan et al. (2018)
Normalized Difference Vegetation Index – NDVI	$(R_n - R_r)/(R_n + R_r)$	Gitelson et al. (2002)
Normalized Difference Red-Edge Vegetation Index – NDVI-RE	$(R_n - R_{RE})/(R_n + R_{RE})$	Gitelson e Merzlyak (1994)
Normalized Green Red Difference – NGRD	$(R_g - R_r)/(R_g + R_r)$	Hamuda et al. (2016)
Red Edge Triangular Vegetation Index - RTVI	$100(R_n - R_{RE}) - 10(R_n - R_g)$	Chen et al. (2010)

Continuation...

Table 2. Continuation.

Vegetation indices	Equation	Reference
Red-Edge Chlorophyll Index – RECI	$(R_r/R_{RE}) - 1$	Gitelson et al. (2003)
Soil Adjusted Vegetation Index – SAVI	$\frac{1,5(R_n - R_r)}{(R_n + R_r + 0,5)}$	Zhong et al. (2019)
Simple Ration of Red and NIR Index - SR	R_r/R_n	Bannari et al. (1995)
Simple Ration of Red and Red Edge Index - SR-RE	R_r/R_{RE}	Gitelson e Merzlyak (1994)
Transformed Chlorophyll Absorption in NIR Index – TCARI	$3[(R_n - R_r) - 0,2(R_n - R_g)(R_n/R_r)]$	Haboudane et al. (2004)
Transformed Chlorophyll Absorption in Red-edge Index – TCARI-RE	$3[(R_{RE} - R_r) - 0,2(R_{RE} - R_g)(R_{RE}/R_r)]$	Daughtry et al. (2000)
Wide Dynamic Range Vegetation Index – WDRVI	$\frac{(0,12R_n) - R_r}{(0,12R_n) + R_r}$	Gitelson (2004)

Spectral reflectance: R_n = near infrared (790 nm); R_g = green (550 nm); R_{RE} = red edge (735 nm); R_r = red (660 nm).

The multispectral indices were estimated using the raster calculator in QGIS v. 3.22 (QGIS..., 2023). The vegetation indices were extracted using the zonal statistics plugin of QGIS v. 3.22 (QGIS..., 2023), through the vector layer consisted of 60 polygons with 1 m² area that were randomly distributed in eight subareas: four for the modeling step and four for the model validation step (Figure 2). The zonal statistics plugin generated a table of attributes (number of pixels, mean, minimum, maximum, median, and standard deviation) for the vegetation indices of each polygon. The attributes were subdivided into six sets of ten polygons, whose mean values were used to generate and validate the models.



Figure 2. Sampled areas used for the generation (A) and validation (B) of prediction models for LAI and SDW of cowpea plants of the cultivar BRS-Inhuma. Embrapa Mid-North, Teresina, PI, Brazil.

p1, p3, p5, and p7 = sampled areas for modeling; p2, p4, p6, and p8 = sampled areas for validation.

The statistical analysis of the data was performed as follows: a) Pearson correlation analysis between the parameters LAI and SDW and the evaluated VIs, focused on pre-selecting the most promising VIs for predicting LAI and SDW; b) linear regression analysis to generate prediction models for LAI and SDW; c) validation of prediction models for LAI and SDW; and d) development of LAI and SDW maps with the most promising prediction models to assess spatial variability in the field.

Spatial variability was analyzed through box plot graphs and histograms, which display the distribution of minimum, mean, maximum, median, and standard deviation values, as well as the proportion of area occupied by each class of LAI, leaf dry weight (LDW), and total dry weight (TDW) in the maps. As the number of replications in the field was not adequate, the same dataset collected in the field for LAI and SDW was used, but with a different VI dataset (Figure 2).

The t-test was applied for Pearson correlation analysis. VIs with $r \geq |0.8|$ in relation to the parameters LAI and SDW were considered promising. Statistical analyses (correlation and linear regression analysis) were performed using in the software RBio (Bhering, 2017). Linear regression models were selected based on the coefficient of determination (R^2) (Eq. 2) and the standard error of estimate (EPE) (Eq. 3). Regression models that presented the highest R^2 and the lowest EPE were considered the best models (Han et al., 2019).

$$R^2 = 1 - \frac{\sum_{i=1}^n (y_i - \hat{y}_i)^2}{\sum_{i=1}^n (y_i - \bar{y})^2} \dots\dots\dots (2)$$

$$EPE = \sqrt{\frac{\sum_{i=1}^n (y_i - \bar{y})^2}{n-1}} / \sqrt{n} \dots\dots\dots (3)$$

where: n is the number of observations, the parameter measured in field; the parameter estimated by the regression models, and the mean of the parameters measured in the field.

The performance of the prediction models was assessed using the coefficient of determination (R^2) (Eq. 2), the root mean square error (RMSE) (Eq. 4), and the normalized RMSE (nRMSE) (Eq. 5) (Yu et al., 2020).

$$RMSE = \sqrt{\frac{1}{n} \sum_{i=1}^n (y_i - \hat{y}_i)^2} \dots\dots\dots (4)$$

$$nRMSE = [RMSE / (y_{max} - y_{min})] \times 100 \dots\dots\dots (5)$$

where: is the maximum and the minimum value of the parameter measured in the field. Models with the highest R^2 and lowest RMSE and nRMSE present better performance for predicting LAI and SDW (Han et al., 2019; Ji et al., 2022).

Results and Discussion

Leaf area index

The leaf area index (LAI) of cowpea plants during the development cycle, estimated as a function of plant LA determined in the laboratory (LAI-Lab) and directly measured in the field by ceptometer (LAI-Cep), is shown in Figure 3A. The LAI curve showed increases from 13 days after sowing (DAS) to 40 DAS, with LAI varying from 0.3 ± 0.06 to 7.2 ± 0.70 (measured in laboratory) and from 0.4 ± 0.05 to 6.8 ± 2.29 (measured in the field with a ceptometer). The deviations of LAI-Cep were higher than those in LAI-Lab due to the variability in the LAI measurement processes in the field and laboratory. LAI decreased after 40 DAS, oscillating from 4.9 ± 0.51 to 3.6 ± 0.23 in the laboratory and from 4.7 ± 1.48 to 2.2 ± 0.39 in the field (Figure 3A). The maximum LAI values were recorded 40 DAS, when the crop canopy reached its full development, regardless of the measurement methodology used.

Souza et al. (2017) evaluated the cowpea cultivar BR3-Tracuateua under rainfed and irrigation conditions in Castanhal, PA, Brazil, and found the highest LAI in the irrigated treatment, with 3.29 ± 0.15 at 48 DAS (2012) and 3.26 ± 0.19 at 50 DAS (2013), during the reproduction stage. Under rainfed conditions, the maximum LAI was 1.75 ± 0.09 in 2012 and 2.84 ± 0.17 in 2013, denoting decreases of approximately 46.8% and 12.9%, respectively, when compared to the irrigated treatment. These results showed that cowpea cannot maintain leaf production when subjected to water stress. The decreases in LAI were probably a survival strategy to reduce leaf transpiration surface (Bastos et al., 2011). The LAI results

found by Souza et al. (2017) was lower than those found in the present study, probably due to differences in the growth habits of the cultivars used and in the availability of water and solar radiation, which directly influenced crop growth (Bastos, 2021).

The variability of LAI between the methodologies used for its determination was evident from 33 to 61 DAS, when there was higher variability for field measurements (1.54 to 1.81, with a maximum of 2.29 at 40 DAS) compared to those found for laboratory measurements (0.45 to 0.32, with a maximum of 0.70 at 40 DAS). In the initial stages (13 at 26 DAS) and the final cycle (61 DAS), the variability of LAI obtained by both methods decreased, with deviations from the mean of 0.06 to 0.54 (LAI-Lab) and 0.05 to 0.45 (LAI-Cep) (Figure 3A).

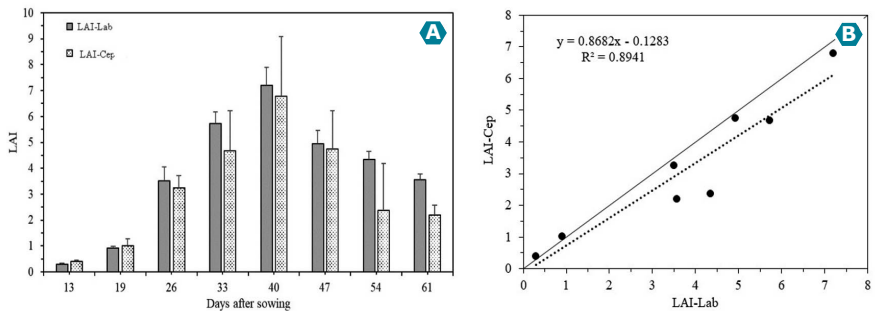


Figure 3. Leaf area index (LAI) of cowpea plants of the cultivar BRS-Inhuma during the development cycle (A), and correlation between leaf areas measured in the laboratory (LAI-Lab) and in the field (LAI-Cep) (B).

The lowest variability of LAI estimated in the laboratory was due to more precise LA measurements by the LAI-3000 device compared to field measurements with the ceptometer device. The ceptometer requires previous configuration with input of empirical values of parameters that affect the performance for LAI readings (Facchi et al., 2010), such as the distribution angle of the crop leaves. This is an important aspect as it affects the estimation of photosynthetically active radiation intercepted by the crop (Accupar..., 2017). Field LAI measurements naturally exhibits leaf overlaps from the upper part over the lower part of the canopy, whereas

in the laboratory, LAI is obtained by summing the area of all plant leaves. Considering the methodological differences for measurement, LAI measured in field by the ceptometer was underestimated by 86.8% ($R^2 = 0.894$) compared to that estimated in the laboratory (Figure 3B). Rodrigues et al. (2013) and Silva et al. (2016) evaluated LAI in grapevine by destructive methods (LI-3100) and in the field (Accupar LP-80) and found that the ceptometer Accupar LP-80 underestimated grapevine LAI in different crop systems, requiring correction for each canopy.

Shoot dry weight

The shoot dry weight (SDW) of cowpea plants during the development cycle is shown in Figure 4. The leaf dry weight varied from $11.5 \pm 0.9 \text{ g m}^{-2}$ at 13 DAS to $235.1 \pm 18.0 \text{ g m}^{-2}$ at 40 DAS, decreasing during the grain maturation stage ($211.5 \pm 5.2 \text{ g m}^{-2}$ at 61 DAS) due to natural leaf senescence (Figure 4A). The stem dry weight exhibited an increasing growth curve from the vegetative stage to maturation, increasing from $7.7 \pm 0.5 \text{ g m}^{-2}$ at 13 DAS to $559.3 \pm 20.9 \text{ g m}^{-2}$ at 61 DAS (Figure 4B). The pod dry weight, concentrated only in the reproduction stage, varied from $1.2 \pm 0.5 \text{ g m}^{-2}$ at 41 DAS to $221.4 \pm 32.7 \text{ g m}^{-2}$ at 54 DAS, at the stages of full pod formation and maturation (Figure 4C).

The aerial part dry weight (leaves, stems, and pods) resulted in a total cumulative dry weight with a typical growth curve, ranging from $19.2 \pm 1.7 \text{ g m}^{-2}$ at 13 DAS to $263.0 \pm 22.8 \text{ g m}^{-2}$ at 33 DAS, at the end of the vegetative stage. A higher increase was found during the reproduction stage due to pod formation and filling, ranging from $578.4 \pm 59.3 \text{ g m}^{-2}$ at 40 DAS to $927.2 \pm 65.6 \text{ g m}^{-2}$ at 54 DAS, at the end of the pod filling stage (Figure 4D).

Souza et al. (2017) evaluated the cowpea cultivar BR3-Tracuateua under rainfed and irrigation conditions in Castanhal, PA, Brazil, and found a similar growth curve for total SDW to that observed in the present study; however, with lower cumulative dry weights. The highest cumulative dry weight obtained was only $538.4 \pm 32.4 \text{ g m}^{-2}$ at 58 DAS in the irrigated crop, which was probably due to differences in the size and growth habit of the cultivars used.

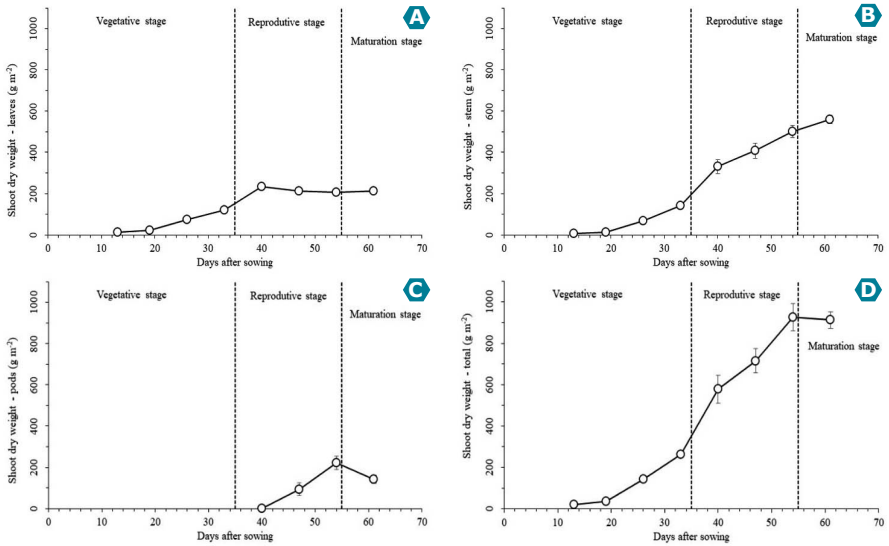


Figure 4. Shoot dry weight of cowpea plants of the cultivar BRS-Inhuma during the development cycle.

(A) Leaves, (B) Stems, (C) Pods, and (D) Total.

Guerra et al. (2020) evaluated the cumulative total SDW of cowpea cultivars at the beginning of flowering under the soil and climate conditions of Barra, western Bahia, Brazil, and found total SDW varying from 360 g m⁻² (BRS-Aracê; 42 days after emergence) to 680 g m⁻² (BRS-Itaim; 31 days after emergence), denoting that biomass production depends on the cultivar's growth habit. The cultivar BRS-Guariba presented a total SDW of 560 g m⁻² at 31 days after emergence (approximately 36 DAS), close to that obtained in the present study (576.3 g m⁻²) for the cultivar BRS-Inhuma at 40 DAS.

Pearson correlation analysis

The Pearson correlation coefficient (r) between the evaluated vegetation indices (VIs) and the field-measured LAI using a ceptometer (LAI-Cep) was higher than that determined in the laboratory (LAI-Lab) in all evaluated situations (Figure 5), denoting that the spectral response of the crop canopy

was better detected by aerial images when the ceptometer was used for measuring LAI. This may be due to the ceptometer's mode of operation, which measure the photosynthetically active radiation above and below the canopy, preserving the natural structure and distribution of canopy leaves; this is the opposite of the laboratory determination, for which the plants are collected in the field, thus changing the canopy structure. As mentioned, LAI measured in the field was underestimated by 86.8% ($R^2 = 0.894$) compared to laboratory measurements, probably due to the methodological differences (Figure 3B) (Rodrigues et al., 2013; Silva et al., 2016).

Considering all eight LAI measurements and the established criterion for selecting the best VIs as those with $r \geq |0.8|$, the VI NDREI ($r = 0.839$, $p < 0.01$), GCI ($r = 0.816$, $p < 0.05$), and gNDVI ($r = 0.812$, $p < 0.05$) stood out for LAI-Lab (Figure 5A); and all others presented $r \geq 0.8$ for LAI-Cep, except NDVI-RE, RDVI, RECI, and SR-RE. NDREI ($r = 0.924$, $p < 0.01$), GCI ($r = 0.912$, $p < 0.01$), TCARI-RE ($r = -0.903$, $p < 0.01$), and gNDVI ($r = 0.901$, $p < 0.01$) presented the highest r values (Figure 5B).

However, considering only the LAI measurements up to the 6th sampling (47 DAS), the number of VIs with $r \geq 0.8$ increased considerably, indicating a higher potential for predicting LAI in cowpea when measurements are taken during the crop reproduction stage (LAI-Cep = 6.8 ± 2.29). The VIs with the highest r values were TCARI-RE ($r = -0.974$, $p < 0.001$), SR ($r = 0.952$, $p < 0.01$), NDREI ($r = 0.951$, $p < 0.01$), and GCI ($r = 0.95$, $p < 0.01$) (Figure 5C) for LAI-Lab measurements; and the most promising VIs ($r \geq 0.8$) were TCARI-RE ($r = 0.95$, $p < 0.001$), NDREI ($r = 0.94$, $p < 0.01$), SR ($r = 0.93$, $p < 0.01$), and GCI ($r = 0.93$, $p < 0.01$) for LAI-Cep measurements (Figure 5D).

According to Haboudane et al. (2004), predicting LAI from spectral image data presents two important challenges: (i) the VI approaches a spectral asymptotic saturation level when $LAI \geq 5 \text{ m}^2 \text{ m}^{-2}$, making it difficult to establishment an acceptable prediction model, depending on the VI used; (ii) there is no single correlation between LAI and a VI, but several correlations depending on leaf chlorophyll content and other characteristics of the crop canopy (Stanton et al., 2017). Kross et al. (2015) found spectral saturation for the VIs gNDVI, NDVI, NDVI-RE, and RTVI when the mean LAI of soybean and maize exceeded $6 \text{ m}^2 \text{ m}^{-2}$.

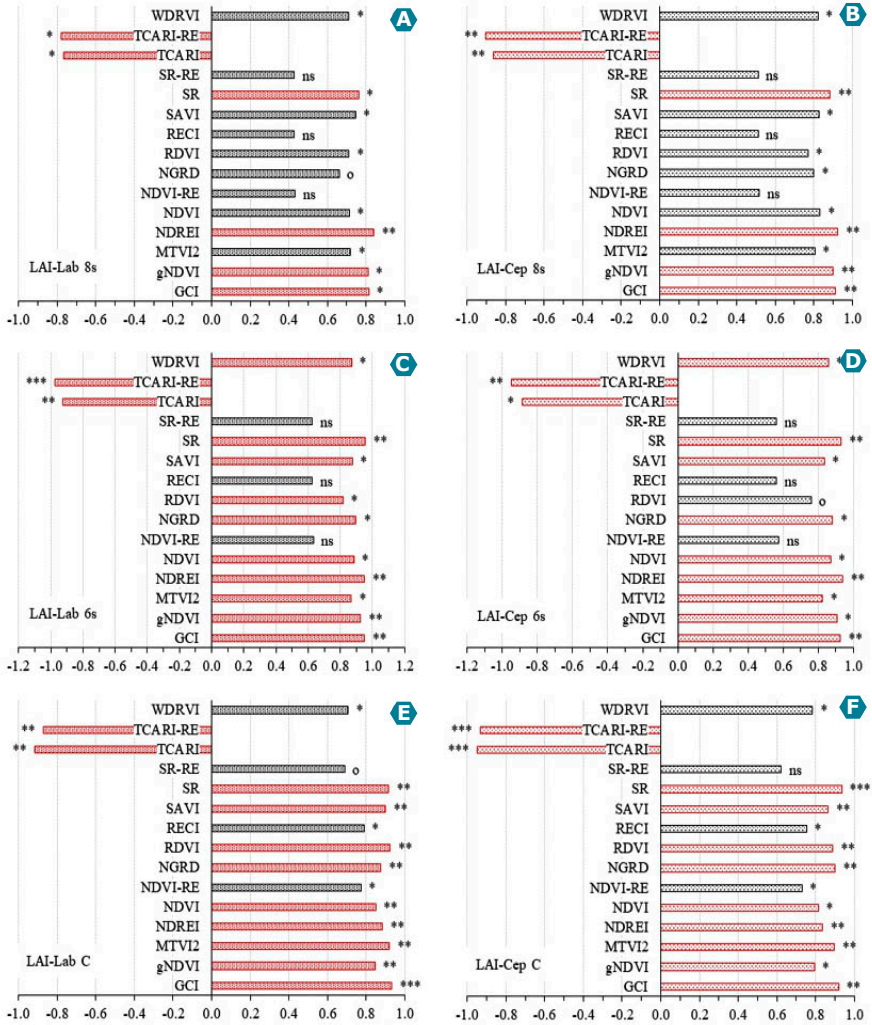


Figure 5. Pearson correlation between LAIs measured in the laboratory (LAI-Lab) and in the field (LAI-Cep) in cowpea plants of the cultivar BRS-Inhuma and the evaluated vegetation indices (VIs).

(A) LAI-Lab and VI measured up to the 8th sampling; (B) LAI-Cep and VI measured up to the 8th sampling; (C) LAI-Lab and VI measured up to the 6th sampling; (D) LAI-Cep and VI measured up to the 6th sampling; (E) LAI-Lab and cumulative VI in successive samplings; (F) LAI-Cep and cumulative VI in successive samplings.

Spectral saturation of VI images was reached after 40 DAS (LAI-Cep = 6.8 ± 2.3), at reproduction stage. Some studies have evaluated and compared several VIs in terms of stability and power for predicting LAI (Baret; Guyot, 1991; Broge; Leblanc, 2000), whereas others have modified some VIs to improve their linearity and increase their sensitivity to LAI (Nemani et al., 1993; Chen, 1996; Brown et al., 2000). Santana et al. (2016) found NDVI saturation for common bean plants 50 days after plant emergence and recommended this vegetation index mainly during the crop vegetative stage. Studies focused on predicting LAI in cowpea plants through VIs from spectral images should advance on finding calibration parameters to reduce the effect of spectral saturation of the promising VIs identified in the present study, as well as incorporate textural information from images that exhibit intrinsic structural and geometric canopy characteristics (Ji et al., 2023).

Using cumulative VI over the cowpea development stages (cumulative VI) was the alternative found for predicting LAI of cowpea crops at any development stage, without the inconvenience of spectral saturation of VI images (Figures 5E and 5F). A similar procedure was used by Kross et al. (2015). In this case, there was a high number of VI with $r \geq |0.8|$ for both methodologies used. The most promising VIs for LAI-Lab were GCI ($r = 0.933$, $p < 0.0001$), RDVI ($r = 0.925$, $p < 0.001$), MTVI2 ($r = 0.92$, $p < 0.001$), and TCARI ($r = -0.918$, $p < 0.01$) (Figure 5E); whereas the most promising VIs for LAI-Cep were TCARI ($r = -0.949$, $p < 0.001$), SR ($r = 0.936$, $p < 0.001$), TCARI-RE ($r = -0.933$, $p < 0.001$), and GCI ($r = 0.918$, $p < 0.01$) (Figure 5F).

Haboudane et al. (2004) searched for methods to minimize the effect of leaf chlorophyll contents on LAI prediction and developed new algorithms that adequately predict canopy LAI for soybean, maize, and wheat crops. They evaluated the performance of existing VIs, such as NDVI, RDVI, SR, SAVI, MSAVI, TVI, and MCARI, and prospected the use of new VIs (MTVI1, MCARI1, MTVI2, and MCARI2) that are less sensitive to chlorophyll content variations and linearly correlated with canopy LAI. They concluded that the existing VIs were sensitive to changes in chlorophyll contents or affected

by spectral saturation at high LAI. However, they developed two spectral indices (MTVI2 and MCARI2) that proved to be the best predictors of LAI for soybean, maize, and wheat crops. The analysis of the prediction power of the proposed algorithms based on MCARI2 and MTVI2 showed consistent results between the model measurement and non-destructive field measurement of LAI, with coefficients of determination (R^2) of 0.98 for soybean, 0.89 for maize, and 0.74 for wheat.

The prediction of cowpea LAI by the two evaluated methodologies (laboratory and ceptometer) presented similar results to MTVI2, presenting $r = 0.92$ ($p < 0.001$) for LAI-Lab and $r = 0.9$ ($p < 0.01$) for LAI-Cep (Figures 5E and 5F). According to Haboudane et al. (2004), MTVI2 has the advantage of being less sensitive to changes in leaf chlorophyll contents. Kross et al. (2015) found that MTVI2 is sensitive to leaf inclination angle in soybean and maize crops, as also found by Liu et al. (2012). Gano et al. (2021) evaluated the performance of VIs (NDVI, CTVI, MSAVI2, gNDVI, and SR) in predicting LAI in sorghum canopies and found that SR and gNDVI are promising for predicting LAI in sorghum plants, with $r = 0.87$ ($p < 0.001$) for both VIs.

The Pearson correlation between total (TDW) and leaf (LDW) dry weights of cowpea plants and the evaluated VIs is shown in Figure 6. The correlation with SDW data measured at all samplings, as well as up to the 6th sampling (47 DAS) was evaluated. TDW presented significant correlation with the evaluated VIs for measurements taken up to the 4th sampling (33 DAS) (vegetative stage); there was no correlation between the VIs with TDW up to the 8th sampling, as well as with cumulative VI (Figures 6A, 6C, and 6E). However, LDW presented correlation with the evaluated VIs for measurements taken up to the 5th sampling (40 DAS) (beginning of the reproduction stage) and with cumulative VI for the successive measurements up to the 8th sampling (Figures 6B, 6D and 6F).

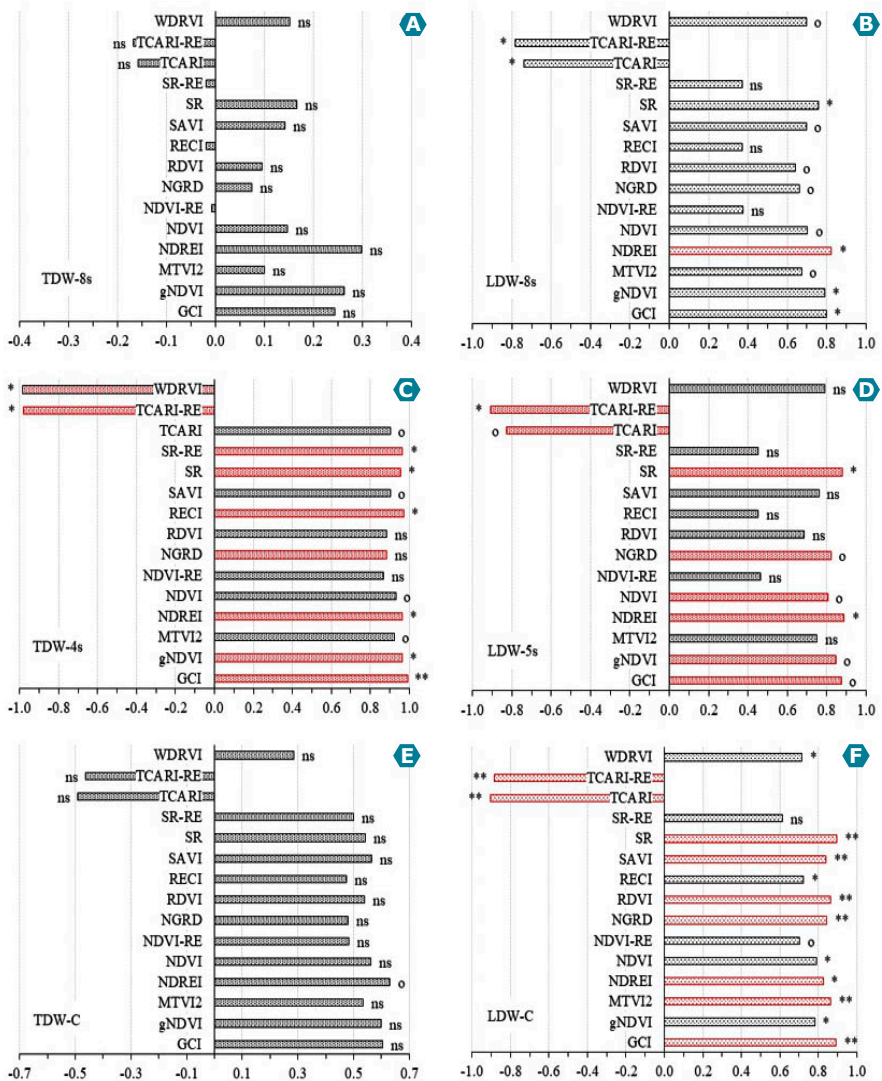


Figure 6. Pearson correlation between total (TDW) and leaf (LDW) dry weights of cowpea plants of the cultivar BRS-Inhuma and the evaluated vegetation indices (VIs).

(A) TDW and VI measured up to the 8th sampling; (B) LDW and VI measured up to the 8th sampling; (C) TDW and VI measured up to the 4th sampling; (D) LDW and VI measured up to the 5th sampling; (E) TDW and cumulative VI in successive samplings; (F) LDW and cumulative VI in successive samplings.

These results denoted spectral saturation of VI for predicting TDW and LDW of cowpea plants at 33 and 40 DAS, respectively, which is equivalent to $263.0 \pm 22.8 \text{ g m}^{-2}$ (TDW) at the end of the vegetative stage and $235.1 \pm 18.0 \text{ g m}^{-2}$ (LDW) at the beginning of the reproduction stage (Figure 4D). Gano et al. (2021) found spectral saturation of VIs (NDVI, CTVI, gNDVI, MSAVI2, and SR) for predicting total dry weight of sorghum when the plants reached 75 g per plant. They explained that this VI spectral saturation is due to decreases in LA after the flowering period. Mutanga e Skidmore (2004) reported that other indices such as NDREI, TCARI-RE, RTVI, and SR-RE may be more efficient in predicting biomass production after canopy closure due to saturation in the Red-Edge spectral band in intermediate and late crop growth stages. Similar LDW results were found in the present study for cowpea plants, which presented a slight decrease in LA after the 5th sampling (40 DAS), during the reproduction stage (Figure 4A).

According to the selection criterion established for the best VIs (those with $r \geq |0.8|$), TCARI-RE ($r = -0.985$, $p < 0.05$), TCARI ($r = -0.982$, $p < 0.05$), RDVI ($r = 0.973$, $p < 0.05$), SR ($r = 0.967$, $p < 0.05$), GCI ($r = 0.963$, $p < 0.05$), and MTVI2 ($r = 0.963$, $p < 0.05$) stood out in predicting TDW (Figure 6C), whereas TCARI-RE ($r = -0.908$, $p < 0.05$), NDREI ($r = -0.890$, $p < 0.05$), SR ($r = 0.881$, $p < 0.05$), GCI ($r = 0.875$, $p < 0.1$), gNDVI ($r = 0.847$, $p < 0.1$), and TCARI ($r = -0.826$, $p < 0.1$) stood out in predicting LDW (Figure 6D). According to Kross et al. (2015), VIs that include spectral reflectance in the Red-Edge band, such as RTVI, NDREI, and TCARI-RE, increase the potential to estimate SDW (Haboudane et al., 2004; Chen et al., 2010).

Ji et al. (2023) evaluated the prediction of total SDW of fava bean through VIs based on RGB images and found that GRVI, NDI, VARI, ExR, and MGRVI presented higher correlation with total SDW ($r = 0.71$ or -0.71) at the reproduction stage, whereas GRVI, NDI, GLI2, VARI, ExR, and MGRVI presented higher correlation with total SDW ($r = 0.62$ or -0.62) at the beginning of grain filling stage. The multispectral images used in the present study encompassed the NIR and Red-Edge bands, allowing for a better assessment of plant spectral responses than images with only red, green, and blue bands (Fei et al., 2021).

Considering the cumulative VI, there was a high number of VI with $r \geq 0.8$. The most promising VIs for LDW were TCARI ($r = -0.905$, $p < 0.01$), SR ($r = 0.896$, $p < 0.01$), GCI ($r = 0.894$, $p < 0.01$), and TCARI-RE ($r = -0.883$, $p < 0.01$) (Figure 6F). Similar results were found for LAI prediction (Figures 5E and F). However, this approach did not prove to be efficient for predicting TDW (Figure 6E). According to Kross et al. (2015), cumulative VI presents good performance for estimating total SDW ($r = -0.883$, $p < 0.01$), mainly for maize crops ($CV \leq 20\%$). Cumulative VI has been used to include absorbed photosynthetically active radiation (Liu et al., 2009), which is proportional to total dry weight (Monteith, 1972). However, in the present study, this alternative was efficient only for leaf dry weight.

Generation of prediction models

The prediction models for LAI-Lab and LAI-Cep obtained with the most promising VIs are shown in Figures 7 and 8, respectively. NDREI and GCI stood out for LAI-Lab, measured up to the 6th and 8th samplings, presenting the best fit to first-order linear models (Figures 7A the 7D). NDREI-8th presented $R^2 = 0.7042$ ($p < 0.01$) and standard error of estimate (EPE) = 0.69 (Figure 7A), whereas GCI-8th presented $R^2 = 0.6653$ ($p < 0.05$) and EPE = 0.67 (Figure 7B). NDREI-6th presented $R^2 = 0.9051$ ($p < 0.01$) and EPE = 1.06 (Figure 7C), whereas GCI-6th presented $R^2 = 0.9029$ ($p < 0.01$) and EPE = 1.03 (Figure 7D). Kross et al. (2015) also found that linear prediction models for LAI of soybean and maize crops presented better fit for the VIs gNDVI ($R^2 = 0.89$), NDVI ($R^2 = 0.89$), NDVI-RE ($R^2 = 0.83$), and RTVI ($R^2 = 0.87$); however, all indices exhibited some spectral saturation when LAI reached $6 \text{ m}^2 \text{ m}^{-2}$. In the present study, spectral saturation occurred from 40 DAS onwards, with a maximum LAI-Cep of 6.8 ± 2.3 and LAI-Lab of $7.2 \pm 0.7 \text{ m}^2 \text{ m}^{-2}$ (reproduction stage) (Figure 3A). This result explains the better fit of LAI prediction models up to the 6th sampling compared to the 8th sampling.

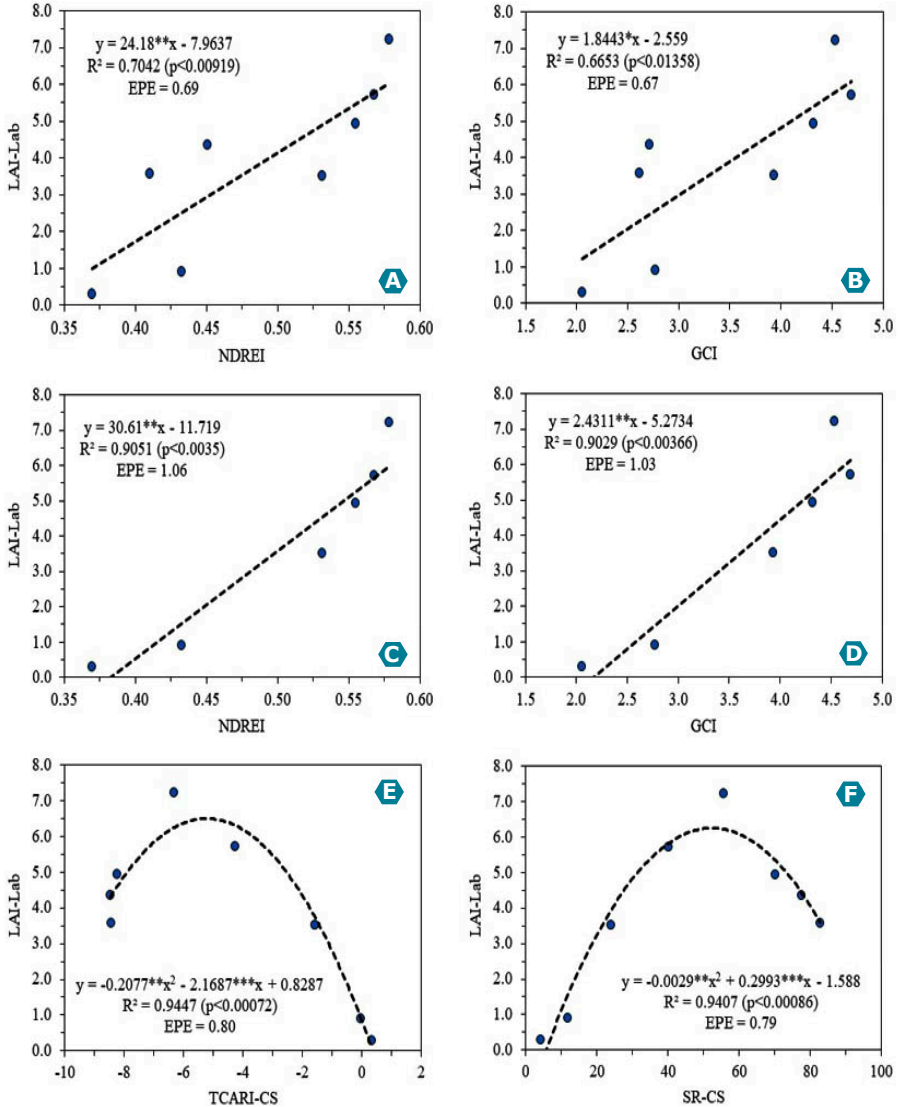


Figure 7. Prediction models for LAI-Lab in canopy of cowpea plants (cultivar BRS-Inhuma) based on the two most promising vegetation indices ($r \geq 0.8$).

(A) NDREI-8th; (B) GCI-8th; (C) NDREI-6th; (D) GCI-6th; (E) TCARI-CS; and (F) SR-CS. 8th = measurements up to the 8th sampling; 6th = measurements up to the 6th sampling; CS = cumulative samplings. Significance levels of model coefficients: * ($p < 0.05$), ** ($p < 0.01$) and *** ($p < 0.001$).

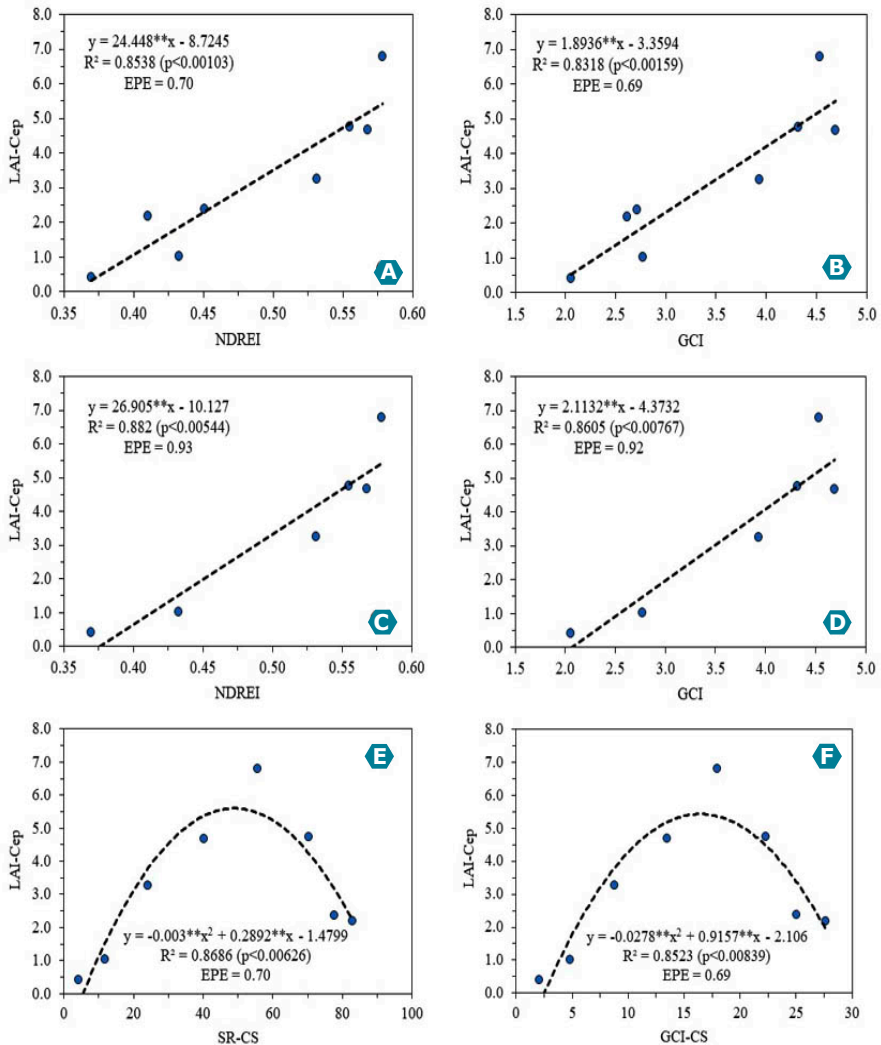


Figure 8. Prediction models for LAI-Cep in canopy of cowpea plants (cultivar BRS-Inhuma) based on the two most promising vegetation indices ($r \geq 0.8$).

(A) NDREI-8th; (B) GCI-8th; (C) NDREI-6th; (D) GCI-6th; (E) SR-CS; and (F) GCI-CS. 8th = measurements up to the 8th sampling; 6th = measurements up to the 6th sampling; CS = cumulative samplings. Significance levels of model coefficients: * ($p < 0.05$), ** ($p < 0.01$) and *** ($p < 0.001$).

According to Gitelson et al. (2014), the best correlations of NDVI with LAI and photosynthetically active radiation occur during the vegetative stage for maize and soybean crops. However, during the reproduction stage, the NDVI presented few changes as a function of LA increases. Similar result was found in the present study.

Santana et al. (2016) evaluated common bean plants and found linear LAI prediction models based on NDVI for four cultivars, in two sowing times. The prediction models presented R^2 of 0.928 (cultivar Agreste), 0.942 (cultivar Perola), 0.893 (cultivar BAT 477), and 0.707 (cultivar BRS-Pontal) for the first sowing time (May 17, 2013).

The LAI prediction models using cumulative VI in cumulative samplings showed a better fit than models using VI measured up to the 6th and 8th samplings. TCARI presented $R^2 = 0.9447$ ($p < 0.001$) and EPE = 0.8, whereas SR presented $R^2 = 0.9407$ ($p < 0.001$) and EPE = 0.79 (Figures 7E and 7F). The prediction models using cumulative TCARI and SR fitted to second-order polynomial functions, denoting that the cumulative VI during the cowpea crop cycle was efficient in overcoming the spectral saturation limitations, enabling the prediction of LAI even after reaching the maximum LAI measured in the field (Kross et al., 2015).

Haboudane et al. (2004) found the best fit for LAI prediction in soybean, maize, and wheat crops using exponential functions, with an R^2 higher than 0.98, and found that the most promising VIs were RDVI, TVI, MSAVI, and MTVI2, as they combine low sensitivity to changes in chlorophyll content and the ability to predict LAI in crops with moderate to high density ($LAI > 3$) (Broge; Leblanc, 2000).

The prediction models of LAI-Cep (Figure 8) and LAI-Lab (Figure 7) presented similar results; however, with better statistical indicators, i.e., higher R^2 and lower EPE, for measurements carried taken up to the 6th sampling, probably due to methodological differences in LAI measurements in the field, resulting in an underestimation of 86.8% ($R^2 = 0.894$) for LA-Cep compared to LA-Lab (Figure 5B).

NDREI and GCI stood out for LAI-Cep measurements up to the 6th and 8th samplings, presenting the best fit to first-order linear models (Figures 8A to 8D). NDREI-8th presented $R^2 = 0.8538$ ($p < 0.01$) and EPE = 0.7 (Figure 8A), whereas GCI-8th presented $R^2 = 0.8318$ ($p < 0.01$) and EPE = 0.69 (Figure 8B). NDREI-6th presented $R^2 = 0.882$ ($p < 0.01$) and EPE = 0.93 (Figure 8C), whereas GCI-6th presented $R^2 = 0.8605$ ($p < 0.01$) and EPE = 0.92 (Figure 8D).

In the predictive models of cumulative LAI, SR stood out with $R^2 = 0.8686$ ($p < 0.01$) and EPE = 0.7 (Figure 8E), followed by GCI with $R^2 = 0.8523$ ($p < 0.01$) and EPE = 0.69 (Figure 8F). The prediction models with cumulative VI fitted to second-order polynomial functions, reinforcing the trend that the cumulative VI strategy is effective in overcoming spectral saturation limitations in cowpea crops, as previous found for soybean, maize, and wheat crops (Kross et al., 2015).

The prediction models of LDW and TDW in cowpea plants are shown in Figures 9 and 10, respectively. The models fitted better to exponential (prediction up to the 5th sampling) and first-order polynomial (cumulative samplings) functions.

The most promising models ($r \geq 0.8$) for leaf dry weight measurements up to the 5th sampling were NDREI-5th, with $R^2 = 0.9091$ ($p < 0.05$) and EPE = 40.5 g m⁻² (Figure 9A), and TCARI-RE-5th, with $R^2 = 0.7541$ ($p < 0.1$) and EPE = 34.1 g m⁻² (Figure 9B). The most promising VIs for the models based on cumulative VI were TCARI-RE, with $R^2 = 0.9325$ ($p < 0.001$) and EPE = 31.3 g m⁻² (Figure 9C), and TCARI, with $R^2 = 0.9238$ ($p < 0.001$) and EPE = 31.1 g m⁻² (Figure 9D).

The most promising models for predicting TDW up to the 4th sampling were generated using gNDVI, with $R^2 = 0.9985$ ($p < 0.01$) and EPE = 56.7 g m⁻² (Figure 10A), and NDREI, with $R^2 = 0.9978$ ($p < 0.01$) and EPE = 57.3 g m⁻² (Figure 10B).

In the prediction models obtained for cumulative VI, SR stood out, with $R^2 = 0.9606$ ($p < 0.001$) and EPE = 132.5 g m⁻² (Figure 10C), followed by GCI, with $R^2 = 0.9668$ ($p < 0.001$) and EPE = 132.3 g m⁻² (Figure 10D). The models fitted better to exponential (prediction up to the 5th sampling) and first-order polynomial (cumulative samplings) functions.

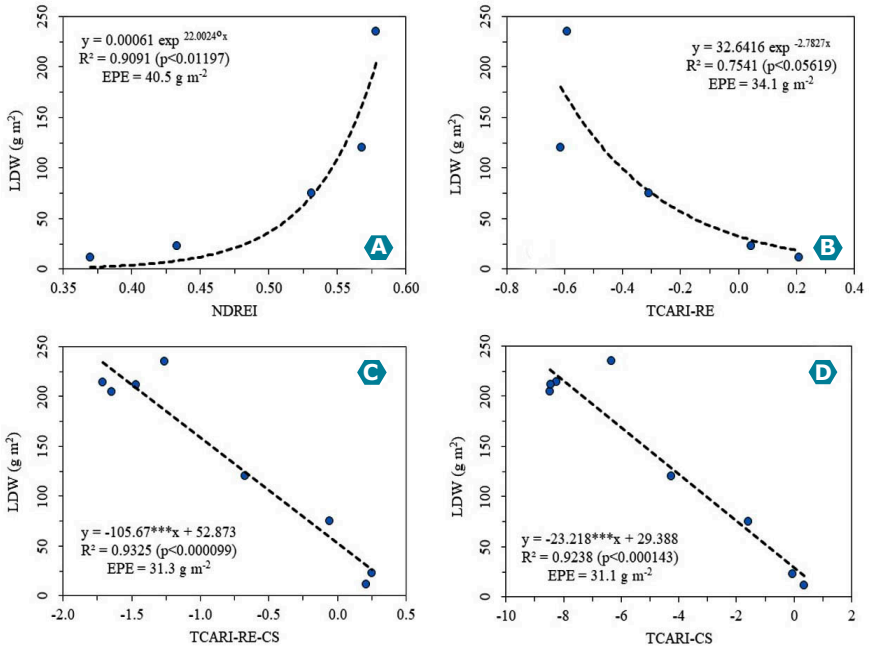


Figure 9. Prediction models for leaf dry weight (LDW) in cowpea plants (cultivar BRS-Inhuma) based on the two most promising vegetation indices ($r \geq 0.8$).

(A) NDREI-5th; (B) TCARI-RE-5th; (C) TCARI-RE-CS; and (D) TCARI-CS. 5th = measurements up to the 5th sampling; CS = cumulative samplings. Significance levels of model coefficients: ° ($p < 0.1$), * ($p < 0.05$), ** ($p < 0.01$) and *** ($p < 0.001$).

Kross et al. (2015) evaluated prediction models for LDW in soybean, maize, and wheat crops and found exponential functions for NDVI ($R^2 = 0.86$), MTVI2 ($R^2 = 0.84$), and gNDVI ($R^2 = 0.82$), whereas the most promising models were linear, for the IVs SR ($R^2 = 0.89$) and RTVI ($R^2 = 0.92$). Regarding TDW, they found an exponential prediction model for NDVI-RE ($R^2 = 0.78$) and a linear model for SR-RE ($R^2 = 0.58$). All indices presented spectral saturation of approximately 400 g m⁻² and 800 g m⁻² for LDW and TDW, respectively. In the present study, the spectral saturation for prediction models for LDW and TDW were 235.1±18.0 g m⁻² (40 DAS) and 263.0±22.8 g m⁻² (33 DAS), respectively.

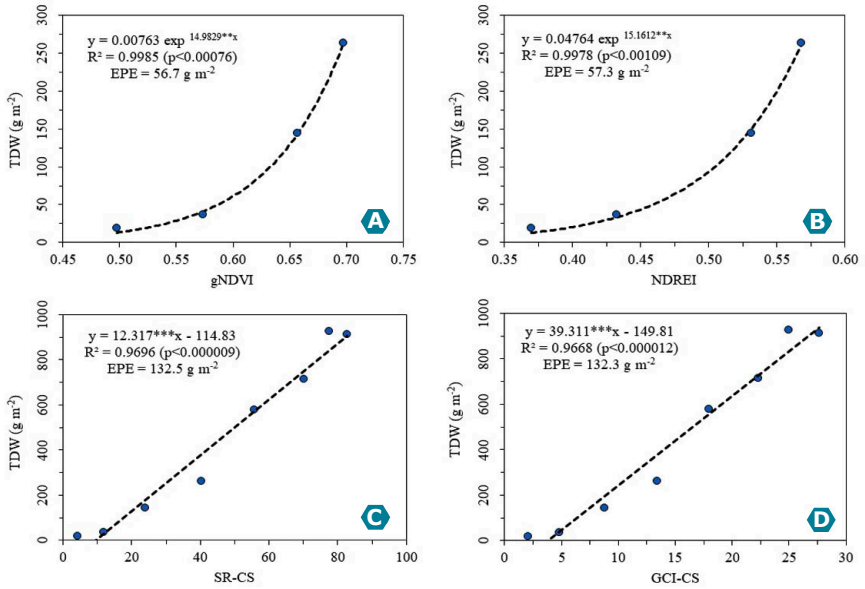


Figure 10. Prediction models for total dry weight (TDW) in cowpea plants (cultivar BRS-Inhuma) based on the two most promising vegetation indices (≥ 0.8).

(A) gNDVI-4th; (B) NDREI-4th; (C) SR-CS; and (D) GCI-CS. 4th = measurements up to the 4th sampling; CS = cumulative samplings. Significance levels of model coefficients: * ($p < 0.05$), ** ($p < 0.01$) and *** ($p < 0.001$).

According to Kross et al. (2015), TDW includes more photosynthetically inactive components (stem and flowers, for instance) than LAI or LDW, which probably affects the correlation between VI and photosynthetically active components. The cumulative VI was a better approach for estimating TDW, with R^2 varying between 0.73 and 0.92 for maize (linear correlations for all VI) and between 0.66 and 0.93 for soybean (linear and exponential correlations).

Gano et al. (2021) defined exponential prediction models for TDW in sorghum crops using NDVI, CTVI, and MSAVI2, which presented $R^2 = 0.66$ ($p < 0.001$), as well as gNDVI, with $R^2 = 0.52$ ($p < 0.001$), which are lower than those obtained in the present study. Santana et al. (2016) defined linear prediction models for LDW in common bean crops using NDVI, which

presented R^2 from 0.874 (cultivar BAT 477) to 0.649 (cultivar BRS Agreste). Considering the LDW results of the four evaluated genotypes, they better fitted to a linear prediction model, with an $R^2 = 0.79$. The spectral saturation was reached with approximately 150 g m^{-2} , which was close to the saturation value found in the present study.

Other VIs such as NDREI, TCARI-RE, RTVI, and SR-RE may be more effective in predicting biomass production after canopy closure, as the saturation in the Red-Edge spectral band occurs in intermediate and late stages of the crop growth (Mutanga; Skidmore, 2004; Kross et al., 2015). Similar LDW result was found in the present study for cowpea, which presented a slight decrease in LA after the 5th sampling (40 DAS), during the reproduction stage (Figure 4A).

Validation of prediction models

The validation of prediction models for LAI, LDW and TDW is shown in Figures 11 to 14. The statistical performance was evaluated by the statistical indicators R^2 , RMSE, and nRMSE. Models with the highest R^2 and the lowest RMSE and nRMSE presented better performance in predicting LAI, LDW and TDW (Han et al., 2019; Ji et al., 2022).

Considering all samplings carried out in the field, the prediction models for LAI-Lab that presented better performance were obtained using the VIs NDREI [$R^2 = 0.7071$ ($p < 0.001$), RMSE = 1.179, and nRMSE = 17.1 %] and GCI [$R^2 = 0.6554$ ($p < 0.05$), RMSE = 1.279, and nRMSE = 18.5%] (Figures 11A and 11B). NDREI stood out for samplings carried out up to the 6th sampling, presenting $R^2 = 0.9568$ ($p < 0.0001$), RMSE = 0.2881, and nRMSE = 4.2 % (Figure 11C), followed by GCI [$R^2 = 0.9088$ ($p < 0.001$), RMSE = 0.821, and nRMSE = 11.9 %] (Figure 11D). TCARI stood out for the cumulative VI in successive samplings over the cowpea cycle, presenting $R^2 = 0.9492$ ($p < 0.0001$), RMSE = 0.499, and nRMSE = 7.2 % (Figure 11E), followed by SR [$R^2 = 0.9336$ ($p < 0.0001$), RMSE = 0.575, and nRMSE = 8.3 %] (Figure 11F).

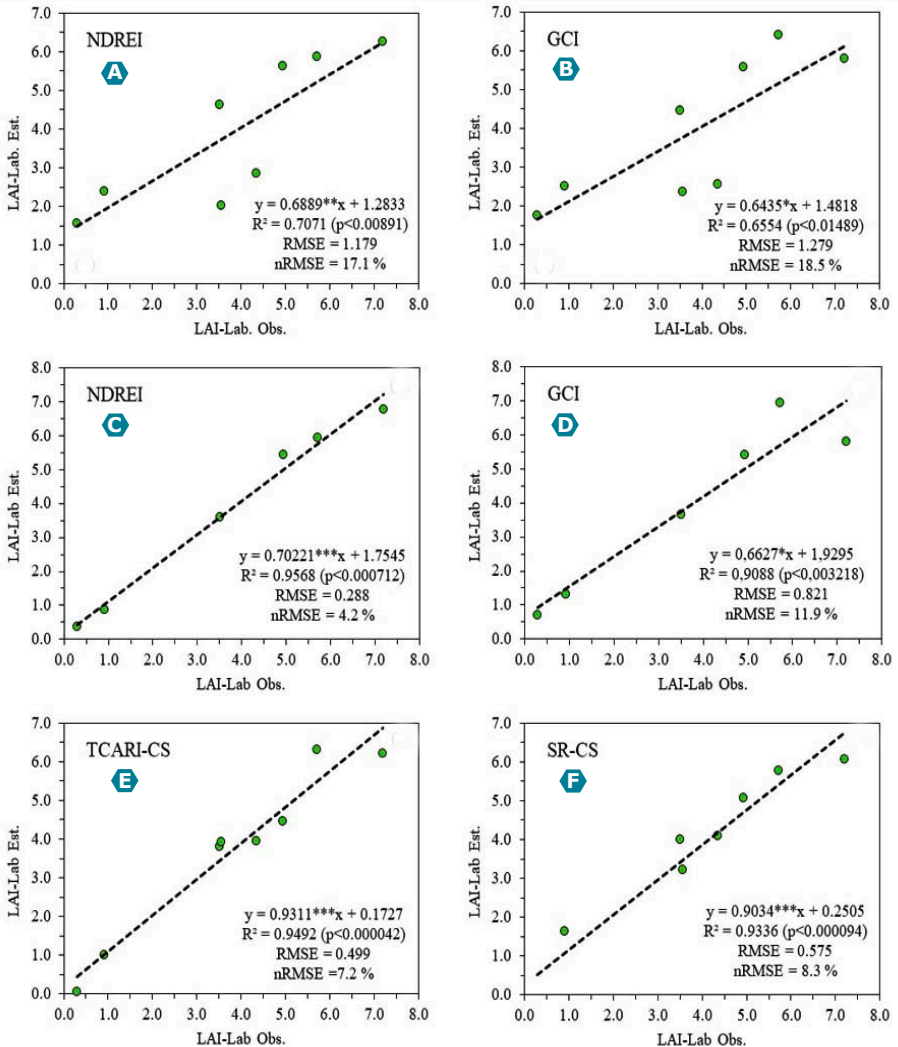


Figure 11. Validation of prediction models for LAI-Lab in canopy of cowpea plants (cultivar BRS-Inhuma) based on the two most promising vegetation indices ($r \geq 0.8$).

(A) NDREI-8th; (B) GCI-8th; (C) NDREI-6th; (D) GCI-6th; (E) TCARI-CS; and (F) SR-CS. 8th = measurements up to the 8th sampling; 6th = measurements up to the 6th sampling; CS = cumulative samplings. Significance levels of model coefficients: * ($p < 0.05$), ** ($p < 0.01$) and *** ($p < 0.001$).

The prediction models for LAI-Cep (Figure 12) presented higher performance (higher R^2 and lower RMSE and nRMSE) than models generated for LAI-Lab (Figure 11), considering all samplings conducted in the field (Figures 12A and 12B).

The best performances when considering all samplings in the field were found for NDREI [$R^2 = 0.8924$ ($p < 0.001$), RMSE = 0.658, and nRMSE = 10.3 %] and GCI [$R^2 = 0.8128$ ($p < 0.001$), RMSE = 0.872, and nRMSE = 13.7%] (Figures 12A and 12B). NDREI stood out for the samplings carried out up to the 6th sampling, presenting $R^2 = 0.9478$ ($p < 0.001$), RMSE = 0.424, and nRMSE = 6.6 % (Figure 12C), as well as GCI [$R^2 = 0.8487$ ($p < 0.001$), RMSE = 0.908, and nRMSE = 14.2 %] (Figure and 12D). GCI stood out for the cumulative VI over the cowpea cycle, with $R^2 = 0.8244$ ($p < 0.001$), RMSE = 1.14, and nRMSE = 16.5% (Figure 12E), as well as SR [$R^2 = 0.8358$ ($p < 0.001$), RMSE = 1.181, and nRMSE = 17.1%] (Figure 12F).

Santana et al. (2016) evaluated the performance of LAI prediction models based on NDVI for four common bean genotypes, in two sowing times. Considering the first sowing time (May 17, 2014), the best fit was found for the genotype Perola ($R^2 = 0.94$; RMSE = 0.31) and the lowest fit quality was found for the genotype BRS Pontal ($R^2 = 0.70$; RMSE = 0.64). Considering the second sowing time (July 03, 2014), the best fit was found for the genotype BAT 477 ($R^2 = 0.99$; RMSE = 0.07) for all quality indicators, whereas the lowest fit quality was found for BRS Agreste ($R^2 = 0.85$; RMSE = 0.24). They found that more prostrated cultivars (BAT 477 and Pérola) performed better for both sowing times, and these cultivars exhibited a more prostrated architecture with a better soil coverage than the BRS Agreste (erect architecture) at the beginning of the crop development cycle, which makes them better for predicting LAI. The cowpea cultivar BRS-Inhuma exhibits an indeterminate growth habit and a semi-prostrate architecture, which may have enabled a better prediction of LAI-Lab and LAI-Cep, mainly for samplings conducted up to the 47 DAS (6th sampling) (Figures 11C, 11D, 12C and 12D).

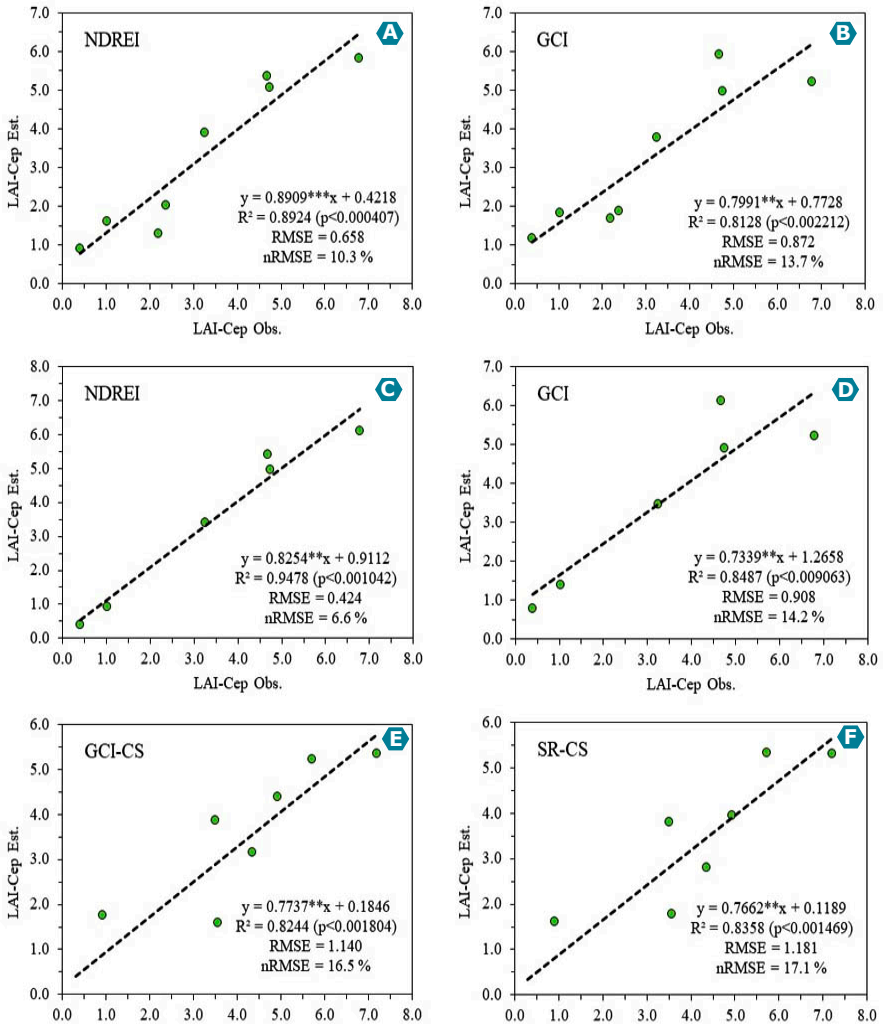


Figure 12. Validation of prediction models for LAI-Cep in canopy of cowpea plants (cultivar BRS-Inhuma) based on the two most promising vegetation indices ($r \geq 0.8$).

(A) NDREI-8th; (B) GCI-8th; (C) NDREI-6th; (D) GCI-6th; (E) GCI-CS; and (F) SR-CS. 8th = measurements up to the 8th sampling; 6th = measurements up to the 6th sampling (47 DAS); CS = cumulative samplings. Significance levels of model coefficients: * ($p < 0.05$), ** ($p < 0.01$) and *** ($p < 0.001$).

Haboudane et al. (2004) evaluated the performance of LAI prediction models for soybean and maize crops using the VIs MTVI2, MSAVI, RDVI, and TVI and found the best predictions of soybean LAI when using MTVI2 ($R^2 = 0.98$; RMSE = 0.28), MSAVI ($R^2 = 0.97$; RMSE = 0.43), and RDVI ($R^2 = 0.95$; RMSE = 0.75); the maize crop showed a slight lower fit for the same VIs: MTVI2 ($R^2 = 0.89$; RMSE = 0.46), MSAVI ($R^2 = 0.88$; RMSE = 0.58), and TVI ($R^2 = 0.81$; RMSE = 1.21). The R^2 and RMSE obtained were very similar to those found in the present study for cowpea plants.

LAI prediction models using cumulative VI during the cowpea development cycle had better performance than the models using simple (non-cumulative) VI for LAI-Lab (Figure 11E and 11F), denoting that the strategy of using cumulative VI was effective in overcoming spectral saturation limitations, allowing for LAI prediction in cowpea crops even after reaching the maximum LAI measured in the field (Kross et al., 2015).

Regarding SDW, the best-performing models for predicting leaf dry weight (LDW) in evaluations carried out up to 40 DAS were NDREI [$R^2 = 0.9964$ ($p < 0.01$), RMSE = 35.0 g m⁻², and nRMSE = 15.7 %] and TCARI-RE [$R^2 = 0.9128$ ($p < 0.1$), RMSE = 40.7 g m⁻², and nRMSE = 18.2 %] (Figures 13A and 13B). The best-performing models for cumulative samplings over the crop cycle were TCARI-RE [$R^2 = 0.93$ ($p < 0.001$), RMSE = 22.7 g m⁻², and nRMSE = 10.2 %] and TCARI [$R^2 = 0.9176$ ($p < 0.001$); RMSE = 24.8 g m⁻², and nRMSE = 11.1 %] (Figures 13C and 13D).

The models that showed the best fit for predicting TDW up to the 4th sampling were obtained using the VIs gNDVI [$R^2 = 0.9954$ ($p < 0.01$), RMSE = 10.0 g m⁻², and nRMSE = 4.1 %] and NDREI [$R^2 = 0.9907$ ($p < 0.01$), RMSE = 12.0 g m⁻², and nRMSE = 4.9 %] (Figures 14A and 14B). The best fit for the prediction models obtained using cumulative VI were found for the VIs SR [$R^2 = 0.9693$ ($p < 0.001$), RMSE = 62.5 g m⁻², and nRMSE = 7.0 %] and GCI [$R^2 = 0.9669$ ($p < 0.001$), RMSE = 65.9 g m⁻², and nRMSE = 7.4 %] (Figures 14C and 14D).

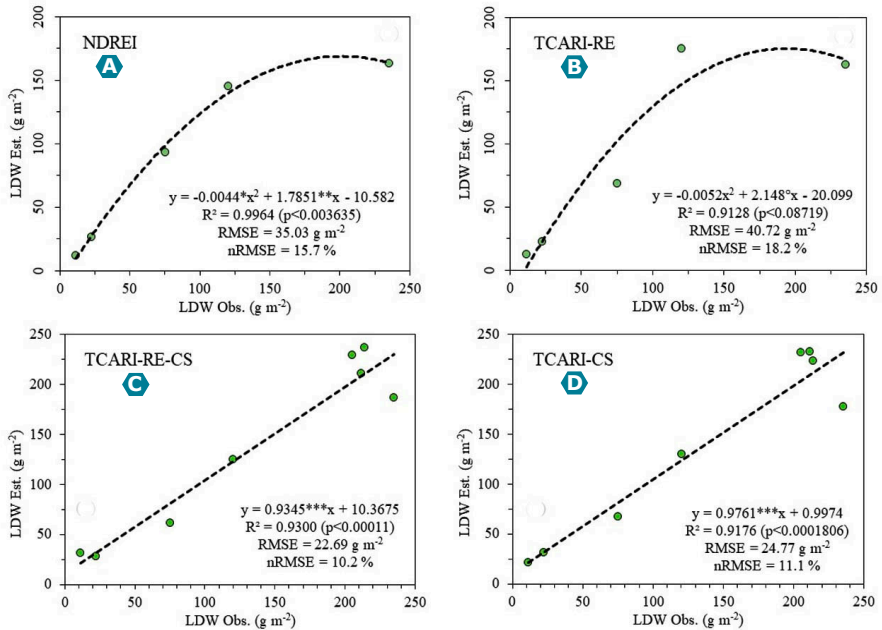


Figure 13. Validation of prediction models for leaf dry weight (LDW) in cowpea plants (cultivar BRS-Inhuma) based on the two most promising vegetation indices ($r \geq |0.8|$).

(A) NDREI-5th; (B) TCARI-RE-5th; (C) TCARI-RE-CS; and (D) TCARI-CS. 5th = measurements up to the 5th sampling (40 DAS); CS = cumulative samplings. Significance levels of model coefficients: ° ($p < 0.1$), * ($p < 0.05$), ** ($p < 0.01$) and *** ($p < 0.001$).

Kross et al. (2015) found best fit for LDW prediction models in soybean and maize crops using the VIs NDVI [$R^2 = 0.9$ ($p < 0.0707$) and mean square error (MSE) = 82.7 g m⁻²] and RTVI [$R^2 = 0.79$ ($p < 0.0021$) and MSE = 130.3 g m⁻²]. The models generated using cumulative MTVI2 stood out for predicting TDW in soybean, presenting $R^2 = 0.95$ and MSE = 84.3 g m⁻², followed by SR ($R^2 = 0.87$ and MSE = 77.8 g m⁻²). Regarding the maize plants, the best performance was found for models using the cumulative Vis SR-RE ($R^2 = 0.97$ and MSE = 101.2 g m⁻²) and NDVI ($R^2 = 0.95$ and MSE = 123.4 g m⁻²).

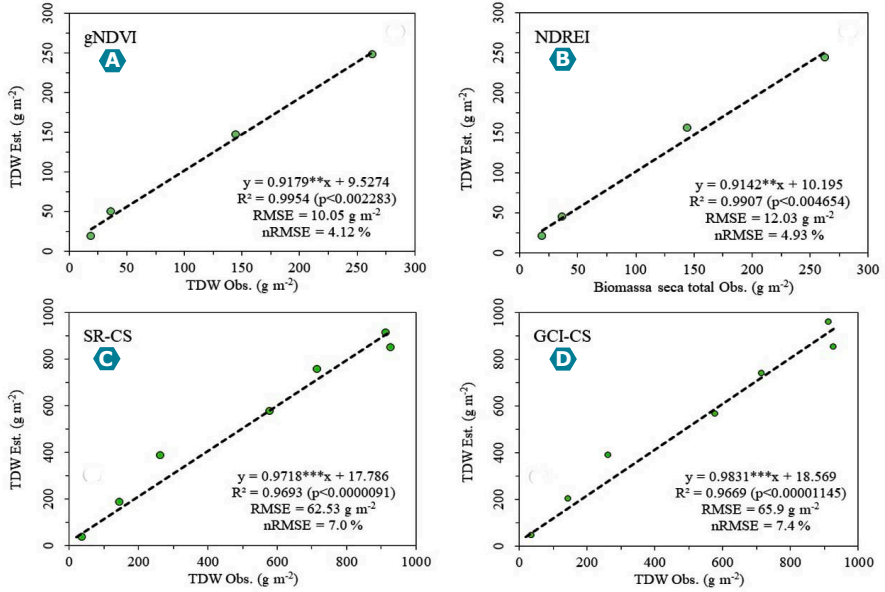


Figure 14. Validation of prediction models for total dry weight (TDW) in cowpea plants (cultivar BRS-Inhuma) based on the two most promising vegetation indices ($r \geq 0.8$).

(A) gNDVI-4th; (B) NDREI-4th; (C) SR-CS; and (D) GCI-CS. 4th = measurements up to the 4th sampling (33 DAS); CS = cumulative samplings. Significance levels of model coefficients: * ($p < 0.05$), ** ($p < 0.01$) and *** ($p < 0.001$).

Gano et al. (2021) found better fit for TDW prediction models in sorghum crops when using the VIs NDVI [$R^2 = 0.91$ ($p < 0.001$) and $RMSE = 4.96 \text{ g plant}^{-1}$], CTVI [$R^2 = 0.92$ ($p < 0.001$) and $RMSE = 4.5 \text{ g plant}^{-1}$], MSAVI2 [$R^2 = 0.92$ ($p < 0.001$) and $RMSE = 4.4 \text{ g plant}^{-1}$], and gNDVI [$R^2 = 0.77$ ($p < 0.001$) and $RMSE = 7.06 \text{ g plant}^{-1}$]. Santana et al. (2016) found better fit for LDW prediction models in common bean crops when using the VIs NDVI ($R^2 = 0.97$, $RMSE = 12, 4 \text{ g m}^{-2}$, and $nRMSE = 12.8 \%$ for the cultivar Agreste; and $R = 0.94$, $RMSE = 8.5 \text{ g m}^{-2}$, and $nRMSE = 10.8 \%$ for the cultivar BAT 477); similar results were obtained in the present study for cowpea regarding the nRMSE of models using cumulative VI (Figures 13C and 13D).

The LDW and TDW prediction models using cumulative VI presented better fit than the individual VI in each stage, which is consistent with the results obtained in the present study (Figures 13C, 13D, 14C and 14D). According to Kross et al. (2015), cumulative VI results in better TDW estimates, as the TDW estimation includes more photosynthetically inactive components (such as stems and flowers) than LAI and LDW, which probably affect the correlation between VI and photosynthetically active components.

Maps of leaf area index and dry weight

The maps of leaf area index (LAI), leaf dry weight (LDW), and total dry weight (TDW) during the cowpea development cycle, obtained with the application of the best-performing prediction models, are shown in Figures 15 to 18. The LAI maps were developed using prediction models based on the VI SR-CS, generated based on LAI measured with a ceptometer (LAI-Cep). Models generated with cumulative VI over the cowpea development cycle were used.

The classes with the highest LAI were found at 33 (a4) and 40 DAS (a5), presenting lower variability (smaller standard deviation), with LAI of 5.1 ± 0.18 (a4) and 5.2 ± 0.10 (a5) when the cowpea reached full vegetative development (Figures 15D and 18A). During this stage, LAI ranged from 5.1 (lower quartile, Q25) to 5.3 (upper quartile, Q75) for the sampling a4 (33 DAS), whereas the sampling a5 (40 DAS) presented LAI ranged from 5.1 (Q25) to 5.2 (Q75), corresponding to 81.7% (a4) and 100% (a5) of the evaluated area (Figure 18D).

A higher LAI variability was found for cowpea plants during the reproduction stage until harvest (a6-a8), which is a period characterized by decreases in leaf growth until complete leaf senescence. Cowpea crops under irrigation are characterized by emission of new leaves, as the adequate water availability in the soil promotes the mixture of plants

with new and senescent leaves in the crop area. During this stage, LAI values were 3.9 ± 0.56 (a6), 3.0 ± 0.70 (a7), and 2.3 ± 0.68 (a8), with percentiles of $Q25 = 3.5$ and $Q75 = 4.3$ (a6), $Q25 = 2.6$ and $Q75 = 3.5$ (a7), and $Q25 = 1.9$ and $Q75 = 2.7$ (a8) (Figure 18A). The distribution of LAI classes in this stage was: 36.7% (LAI = 3.6 to 4.2) and 25.0% (LAI = 4.2 to 4.8) for the sampling a6; 31.7% (LAI = 2.4 to 3.0), 16.7% (LAI = 1.8 to 2.4), and 13.3% (LAI = 3.6 to 4.2) for the sampling a7; and 38.3% (LAI = 1.8 to 2.4), 25.0% (LAI = 2.4 to 3.0), and 20.0% (LAI = 1.2 to 1.8) for the sampling a8 (Figure 18D).

The classes with the highest LDW were found at 47 DAS (a6), corresponding to the end of the vegetative stage, presenting slight decreases at 51 (a7) and 61 (a8) DAS, during the pod maturation stage when natural senescence of cowpea leaves occurs (Figures 16E, 16F, and 16G). LDW variability was higher during these three stages: $LDW = 227.1 \pm 40.3 \text{ g m}^{-2}$ (a6), $LDW = 217.9 \pm 42.0 \text{ g m}^{-2}$ (a7), and $LDW = 199.6 \pm 41.7 \text{ g m}^{-2}$ (a8) (Figure 18B). The sampling a6 (47 DAS) presented LDW ranged from 199.5 g m^{-2} (Q25) to 258.3 g m^{-2} (Q75), whereas the sampling a7 (51 DAS) presented LDW ranged from 184.4 g m^{-2} (Q25) and 250.5 g m^{-2} (Q75); and a8 (61 DAS) presented LDW ranged from 167.0 g m^{-2} to 229.0 g m^{-2} (Figure 18B). The distribution of LDW classes was: 20.0% ($LDW = 220.0$ to 240.0 g m^{-2}), 19.0 % ($LDW = 240.0$ to 280.0 g m^{-2}), and 13.0% ($LDW = 160.0$ to 200.0 g m^{-2}) for the sampling a6; 22.0% ($LDW = 200.0$ to 240.0 g m^{-2}), 17.0% ($LDW = 160.0$ to 200.0 g m^{-2}), and 13.00% ($LDW = 240.0$ to 280.0 g m^{-2}) for the sampling a7; and 19.0% ($LDW = 160.0$ to 200.0 g m^{-2}), 19.0 % ($LDW = 200.0$ to 240.0 g m^{-2}), and 12.0% ($LDW = 240.0$ to 280.0 g m^{-2}) for the sampling a8 (Figure 18E).

Total dry weight (TDW) presented a similar trend to LDW, however, with no TDW decreases during the maturation stage when there is a substitution of leaf dry biomass by pod and grain dry biomasses. The

classes with the highest TDW were found at 51 (a7) and 61 DAS (a8), during the cowpea grain filling and pod maturation stages (Figures 17F and 17G).

TDW variability was higher for the samplings a6 (TDW = 730.5 ± 64.3 g m⁻²) and a7 (TDW = 816.4 ± 64.2 g m⁻²), followed by sampling a8 (TDW = 881.4 ± 59.6 g m⁻²) (Figures 17E, 17F and 17G). TDW ranged from 685.3 g m⁻² (Q25) to 784.7 g m⁻² (Q75) for the sampling a6 (47 DAS); 773.6 g m⁻² (Q25) to 859.6 g m⁻² (Q75) for the sampling a7 (51 DAS); and 848.3 g m⁻² to 917.7 g m⁻² for a8 (61 DAS) (Figure 18C). The distribution of TDW classes was: 36.0% (TDW = 720.0 to 840.0 g m⁻²) and 22.0% (TDW = 600.0 to 720.0 g m⁻²) for the sampling a6; 30.0% (TDW = 720.0 to 840.0 g m⁻²) and 26.0% (TDW = 840.0 to 960.0 g m⁻²) for a7; and 43.0% (TDW = 840.0 to 960.0 g m⁻²) and 13.0% (LDW = 720.0 to 840.0 g m⁻²) for a8 (Figure 18F).

The maps of LAI and dry weights of cowpea plants indicated a relative spatial variability in the evaluated experimental area, which could be utilized due to the excellent statistical performance of the prediction models generated using the cumulative VIs SR (LAI and TDW) and TCARI-RE (LDW), denoting the potential application of prediction models. Further studies are recommended for model validation in agricultural production fields using larger sample areas.

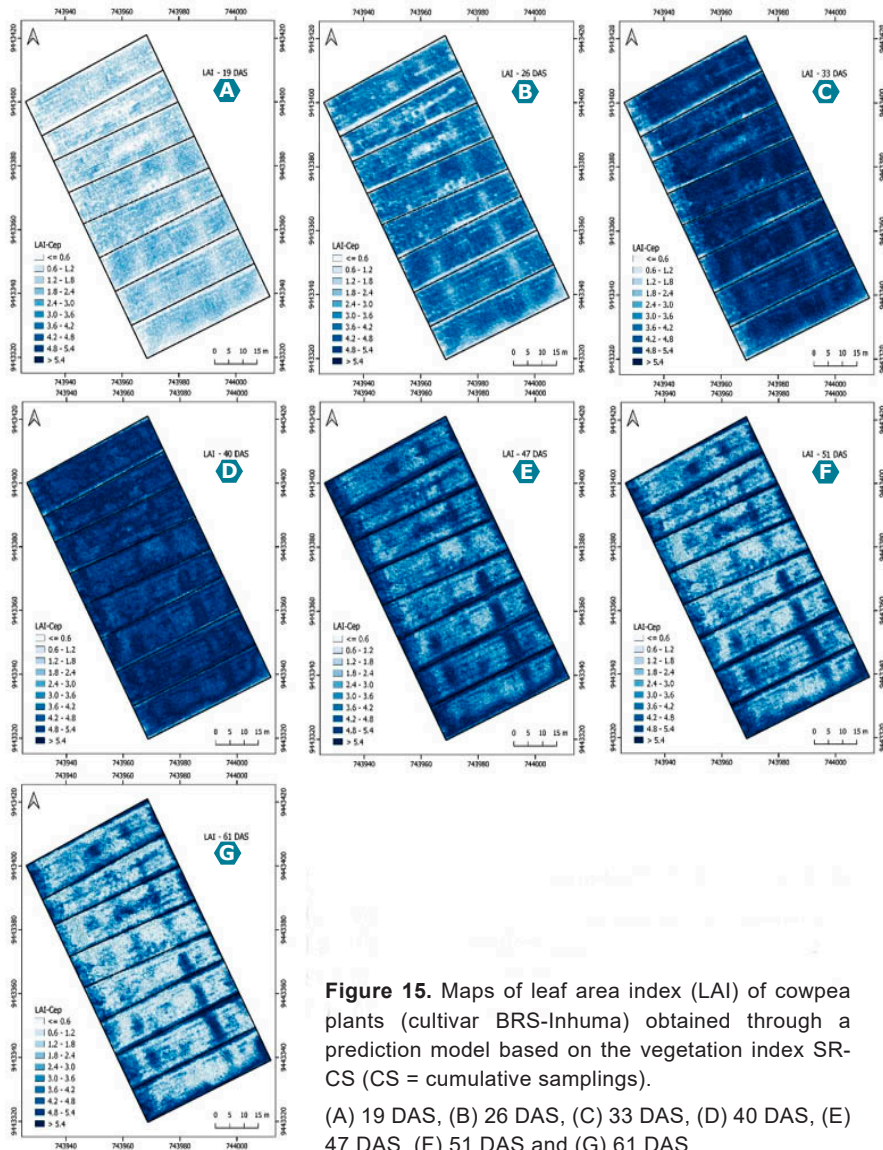


Figure 15. Maps of leaf area index (LAI) of cowpea plants (cultivar BRS-Inhuma) obtained through a prediction model based on the vegetation index SR-CS (CS = cumulative samplings). (A) 19 DAS, (B) 26 DAS, (C) 33 DAS, (D) 40 DAS, (E) 47 DAS, (F) 51 DAS and (G) 61 DAS.

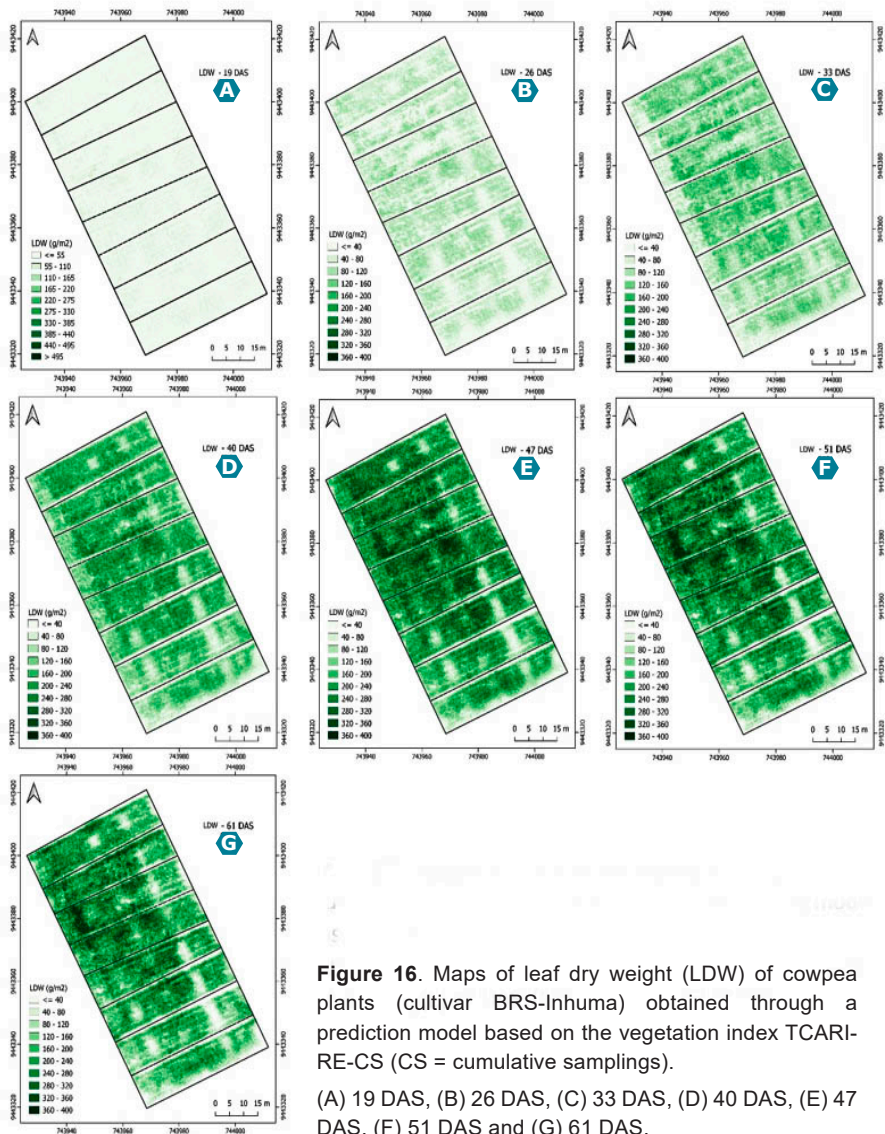


Figure 16. Maps of leaf dry weight (LDW) of cowpea plants (cultivar BRS-Inhuma) obtained through a prediction model based on the vegetation index TCARI-RE-CS (CS = cumulative samplings).

(A) 19 DAS, (B) 26 DAS, (C) 33 DAS, (D) 40 DAS, (E) 47 DAS, (F) 51 DAS and (G) 61 DAS.

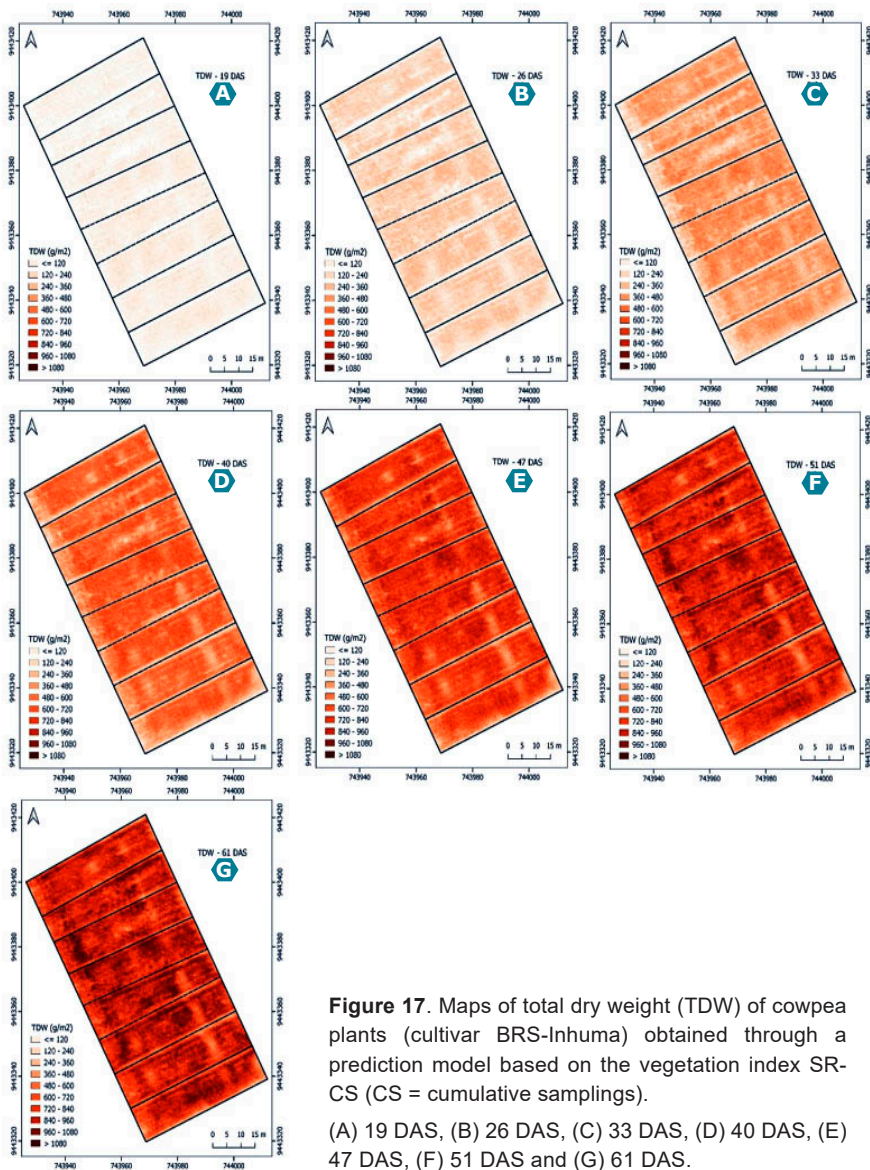


Figure 17. Maps of total dry weight (TDW) of cowpea plants (cultivar BRS-Inhuma) obtained through a prediction model based on the vegetation index SR-CS (CS = cumulative samplings).

(A) 19 DAS, (B) 26 DAS, (C) 33 DAS, (D) 40 DAS, (E) 47 DAS, (F) 51 DAS and (G) 61 DAS.

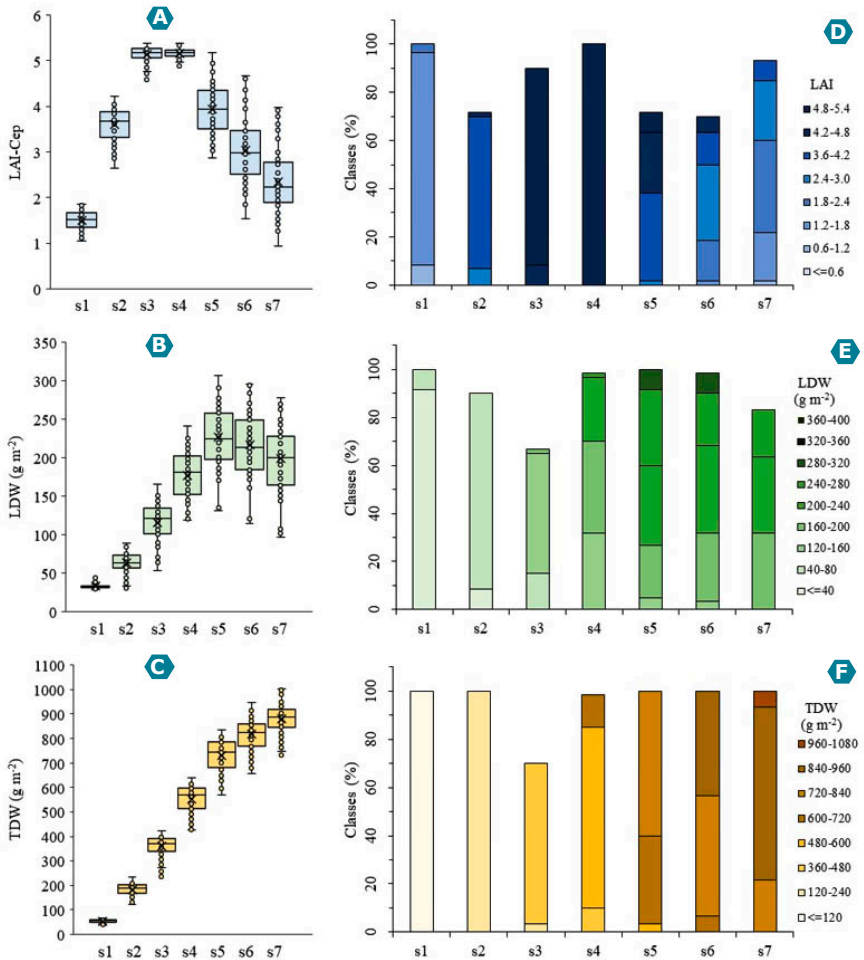


Figure 18. Box plot and histogram of maps of leaf area index (LAI) (A, D), leaf dry weight (LDW) (B, E) and total dry weight (TDW) (C, F) of cowpea plants (cultivar BRS-Inhuma), obtained through prediction models based on the cumulative vegetation indices SR-CS (LAI and TDW) and TCARI-RE-CS (LDW).

(s1) 19 DAS, (s2) 26 DAS, (s3) 33 DAS, (s4) 40 DAS, (s5) 47 DAS, (s6) 51 DAS and (s7) 61 DAS. In each sampling n = 60. CS = cumulative samplings.

Conclusions

- a) Models based on cumulative vegetation indices from multispectral aerial images showed to be promising in predicting leaf area index and shoot dry weight (leaves and total) of cowpea crops;
- b) Quadratic polynomial models based on the cumulative vegetation indices GCI and SR enabled the prediction of leaf area index throughout the cowpea crop cycle, with mean errors of 16.5% and 17.1%, respectively, compared to leaf area index measured in the field with a ceptometer;
- c) Linear models using the cumulative vegetation indices TCARI-RE and TCARI are promising for predicting cowpea leaf dry weight, with mean errors of 22.7 g m^{-2} (10.2%) and 24.8 g m^{-2} (11.1%), respectively, compared to field-measured leaf dry weight;
- d) Linear models using the cumulative vegetation indices SR and GCI are promising for predicting cowpea total dry weight, with mean errors of 62.5 g m^{-2} (7.0%) and 65.9 g m^{-2} (7.4%), respectively, compared to field-measured total dry weight.

References

- ACCUPAR PAR/LAI ceptometer: model LP-80: operator's manual. Pullman: Decagon Devices, 2017. 78 p. Disponível em: http://www.misure.net/sites/default/files/pdf/LP-80_Manual.pdf. Acesso em: 18 mar. 2023.
- ALLEN, R. G.; PEREIRA, L. S.; RAES, D.; SMITH, M. **Crop evapotranspiration: guidelines for computing crop water requirements**. Rome: FAO, 1998. 300p. (FAO. Irrigation and Drainage Paper, 56).
- ANDRADE JUNIOR, A. S. de; LOPES, A. da S.; BASTOS, E. A.; CARDOSO, M. J.; SOUSA, R. C. M. de. **Estimativa da biomassa de milho por imagens RGB de drones**. Teresina: Embrapa Meio-Norte, 2021. 44 p. (Embrapa Meio-Norte. Boletim de pesquisa e desenvolvimento, 140).
- BANNARI, A.; MORIN, D.; BONN, F.; HUETE, A. A review of vegetation indices. **Remote Sensing Reviews**, v. 13, n. 1-2, p. 95-120, 1995.
- BARET, F.; GUYOT, G. Potentials and limits of vegetation indices for LAI and APAR assessment. **Remote Sensing of Environment**, v. 35, n. 2-3, p. 161-173, 1991.
- BASTOS, E. A. Clima. In: RIBEIRO, V. Q. (ed.). **Árvore do conhecimento: feijão-caupi**. Brasília, DF: Embrapa, 2021. Disponível em: <https://www.embrapa.br/agencia-de-informacao-tecnologica/cultivos/feijao-caupi/pre-producao/caracteristicas-e-relacoes-com-o-ambiente/clima>. Acesso em: 18 mar. 2023.
- BASTOS, E. A.; ANDRADE JUNIOR, A. S. de. **Boletim agrometeorológico de 2018 para o município de Teresina, PI**. Teresina: Embrapa Meio-Norte, 2019. 37 p. (Embrapa Meio-Norte. Documentos, 266).
- BASTOS, E. A.; NASCIMENTO, S. P. do; SILVA, E. M. da; FREIRE FILHO, F. R.; GOMIDE, R. L. Identification of cowpea genotypes for drought tolerance. **Revista Ciência Agrônômica**, v. 42, n. 1, p. 100-107, jan./mar. 2011.
- BENDIG, J.; YU, K.; AASEN, H.; BOLTEN, A.; BENNERTZ, S.; BROSCHEIT, J.; GNYP, M. L.; BARETH, G. Combining UAV-based plant height from crop surface models, visible, and near infrared vegetation indices for biomass monitoring in barley. **International Journal of Applied Earth Observation and Geoinformation**, v. 39, p. 79-87, July 2015.
- BHERING, L. L. R. Bio: a tool for biometric and statistical analysis using the R platform. **Crop Breeding and Applied Biotechnology**, v. 17, n. 2, p. 187-190, June 2017.
- BROGE, N. H.; LEBLANC, E. Comparing prediction power and stability of broadband and hyperspectral vegetation indices for estimation of green leaf area index and canopy chlorophyll density. **Remote Sensing of Environment**, v. 76, n. 2, p. 156-172, 2001.

BROWN, L.; CHEN, J. M.; LEBLANC, S. G.; CIHLAR, J. A shortwave infrared modification to the simple ratio for LAI retrieval in boreal forests: An image and model analysis. **Remote Sensing of Environment**, v. 71, n. 1, p. 16-25, 2000.

CHEN, J. M. Evaluation of vegetation indices and modified simple ratio for boreal applications. **Canadian Journal of Remote Sensing**, v. 22, n. 3, p. 229-242, 1996.

CHEN, P. F.; NICOLAS, T.; WANG, J. H.; PHILIPPE, V.; HUANG, W. J.; LI, B. G. New index for crop canopy fresh biomass estimation. **Spectroscopy and Spectral Analysis**, v. 30, n. 2, p. 512-517, 2010.

DAUGHTRY, C. S. T.; WALTHALL, C. L.; KIM, M. S.; DE COLSTOUN, E. B.; MCMURTREY III, J. E. Estimating corn leaf chlorophyll concentration from leaf and canopy reflectance. **Remote Sensing of Environment**, v. 74, n. 2, p. 229-239, 2000.

FACCHI, A.; BARONI, G.; BOSCHETTI, M.; GANDOLFI, C. Comparing optical and direct methods for leaf area index determination in a maize crop. **Journal of Agricultural Engineering**, v. 1, n. 1, p. 33-40, 2010.

FEI, S.; HASSAN, M. A.; HE, Z.; CHEN, Z.; SHU, M.; WANG, J.; LI, C.; XIAO, Y. Assessment of ensemble learning to predict wheat grain yield based on UAV-multispectral reflectance. **Remote Sensing**, v. 13, n. 12, p. 23-38, 2021.

FEIJÃO. **Acompanhamento da Safra Brasileira [de] Grãos**: safra 2022/2023: décimo levantamento, v. 10, n. 10, p. 42-59, jul. 2023. Disponível em: <https://www.conab.gov.br/info-agro/safra/safra/graos/boletim-da-safra-de-graos>. Acesso em: 25 jul. 2023.

FREIRE FILHO, F. R. (ed.). **Feijão-caupi no Brasil**: produção, melhoramento genético, avanços e desafios. Teresina: Embrapa Meio-Norte, 2011. 84 p.

GANO, B.; DEMBELE, J. S. B.; NDOUR, A.; LUQUET, D.; BEURIER, G.; DIOUF, D.; AUDEBERT, A. Using UAV borne, multi-spectral imaging for the field phenotyping of shoot biomass, leaf area index and height of West African sorghum varieties under two contrasted water conditions. **Agronomy**, v. 11, n. 5, p. 850-870, 2021.

GITELSON, A. A. Wide dynamic range vegetation index for remote quantification of biophysical characteristics of vegetation. **Journal of Plant Physiology**, v. 161, n. 2, p. 165-173, 2004.

GITELSON, A. A.; GRITZ, Y.; MERZLYAK, M. N. Relationships between leaf chlorophyll content and spectral reflectance and algorithms for non-destructive chlorophyll assessment in higher plant leaves. **Journal of Plant Physiology**, v. 160, n. 3, p. 271-282, 2003.

GITELSON, A. A.; KAUFMAN, Y. J.; STARK, R.; RUNDQUIST, D. Novel algorithms for remote estimation of vegetation fraction. **Remote Sensing of Environment**, v. 80, n. 1, p. 76-87, 2002.

GITELSON, A. A.; MERZLYAK, M. N. Remote sensing of chlorophyll concentration in higher plant leaves. **Advances in Space Research**, v. 22, n. 5, p. 689-692, 1998.

GITELSON, A.; MERZLYAK, M. N. Spectral reflectance changes associated with autumn senescence of *Aesculus hippocastanum* L. and *Acer platanoides* L. leaves: spectral features and relation to chlorophyll estimation. **Journal of Plant Physiology**, v. 143, n. 3, p. 286-292, 1994.

GITELSON, A. A.; PENG, Y.; HUENNRICH, K. F. Relationship between fraction of radiation absorbed by photosynthesizing maize and soybean canopies and NDVI from remotely sensed data taken at close range and from MODIS 250 m resolution data. **Remote Sensing of Environment**, v. 147, n. 5, p. 108-120, 2014.

GUERRA, A. M. N. de M.; EVANGELISTA, R. S.; SANTOS, E. B. dos; SILVA, M. G. M.; NOGUEIRA, W. P. Produtividade de grãos e de biomassa da parte aérea de cultivares de feijão-caupi. **Revista Agrária Acadêmica**, v. 3, n. 3, p. 40-48, maio/jun. 2020.

HABOUDANE, D.; MILLER, J. R.; PATTEY, E.; ZARCO-TEJADA, P. J.; STRACHAN, I. B. Hyper-spectral vegetation indices and novel algorithms for predicting green LAI of crop canopies: modeling and validation in the context of precision agriculture. **Remote Sensing of Environment**, v. 90, n. 3, p. 337-352, 2004.

HAMUDA, E.; GLAVIN, M.; JONES, E. A survey of image processing techniques for plant extraction and segmentation in the field. **Computers and Electronics in Agriculture**, v. 125, p. 184-199, Jul. 2016.

HAN, L.; YANG, G.; DAI, H.; XU, B.; YANG, H.; FENG, H.; LI, Z.; YANG, X. Modeling maize above-ground biomass based on machine learning approaches using UAV remote-sensing data. **Plant Methods**, v. 15, Article number 10, 2019. 19 p. DOI: 10.1186/s13007-019-0394-z.

HASSAN, M. A.; YANG, M.; RASHEED, A.; JIN, X.; XIA, X.; XIAO, Y.; HE, Z. Time-series multispectral indices from unmanned aerial vehicle imagery reveal Senescence Rate in Bread Wheat. **Remote Sensing**, v. 10, n. 6, p. 809-818, 2018.

Ji, Y.; CHEN, Z.; CHENG, Q.; LIU, R.; LI, M.; YAN, X.; LI, G.; WANG, D.; FU, L.; MA, Y.; JIN, X.; ZONG, X.; YANG, T. Estimation of plant height and yield based on UAV imagery in faba bean (*Vicia faba* L.). **Plant Methods**, v. 18, n. 1, Article number 26, 2022. 13 p. DOI: 10.1186/s13007-022-00861-7.

Ji, Y.; LIU, R.; XIAO, Y.; CUI, Y.; CHEN, Z.; ZONG, X.; YANG, T. Faba bean above-ground biomass and bean yield estimation based on consumer-grade unmanned aerial vehicle RGB images and ensemble learning. **Precision Agriculture**, v. 24, n. 4, p. 1439-1460, 2023.

KROSS, A.; MCNAIRN, H.; LAPEN, D.; SUNOHARA, M.; CHAMPAGNE, C. Assessment of RapidEye vegetation indices for estimation of leaf area index and biomass in corn

and soybean crops. **International Journal of Applied Earth Observation and Geoinformation**, v. 34, p. 235-248, Feb. 2015.

LIU, J.; PATTEY, E.; JÉGO, G. Assessment of vegetation indices for regional crop green LAI estimation from Landsat images over multiple growing seasons. **Remote Sensing of Environment**, v. 123, p. 347-358, Aug. 2012.

LIU, J.; PATTEY, E.; SHANG, J.; ADMIRA, S.; JÉGO, G.; McNAIRN, H.; SMITH, A.; HU, B.; ZHANG, F.; FREEMENTLE, J. Quantifying crop biomass accumulation using multi-temporal optical remote sensing observations. In: CANADIAN SYMPOSIUM ON REMOTE SENSING, 30th., Lethbrigde, 2009. **Proceedings...** Lethbrigde: Canadian Remote Sensing Society: University of Lethbrigde, 2009. p. 22-25.

MELO, F. de B.; ANDRADE JUNIOR, A. S. de; PESSOA, B. L. de O. **Levantamento, zoneamento e mapeamento pedológico detalhado da área experimental da Embrapa Meio-Norte em Teresina, PI**. 2. ed. Teresina: Embrapa Meio-Norte, 2019. 41 p. (Embrapa Meio-Norte. Documentos, 265).

MELO, F. de B.; CARDOSO, M. J.; BASTOS, E. A.; RIBEIRO, V. Q. **Recomendação de adubação e calagem para o feijão-caupi na região Meio-Norte do Brasil**. Teresina: Embrapa Meio-Norte, 2018. 8 p. (Embrapa Meio-Norte. Comunicado técnico, 249).

MONTEITH, J. L. Solar radiation and productivity in tropical ecosystems. **Journal of Applied Ecology**, v. 9, n. 3, p. 747-766, 1972.

MULLA, D. J. Twenty-five years of remote sensing in precision agriculture: key advances and remaining knowledge gaps. **Biosystems Engineering**, v. 114, n. 4, p. 358-371, 2013.

MUTANGA, O.; SKIDMORE, A. K. Narrow band vegetation indices overcome the saturation problem in biomass estimation. **International Journal of Remote Sensing**. v. 25, n. 19, p. 3999-4014, 2004.

NEMANI, R.; PIERCE, L.; RUNNING, S.; BAND, L. Forest ecosystem processes at the watershed scale: sensitivity to remotely-sensed leaf area index estimates. **International Journal of Remote Sensing**, v. 14, n. 13, p. 2519-2534, 1993.

QGIS desktop 3.22 user guide: QGIS project. Boston: Free Software Foundation, dez. 2023. 1419 p. Disponível em: https://docs.qgis.org/3.22/pdf/pt_BR/QGIS-3.22-DesktopUserGuide-pt_BR.pdf. Acesso em: 18 mar. 2023.

QUILLE-MAMANI, J.; PORRAS-JORGE, R.; SARAVIA-NAVARRO, D.; HERRERA, J.; CHÁVEZ-GALARZA, J.; ARBIZU, C.I.; VALQUI-VALQUI, L. Assessment of vegetation indices derived from UAV images for predicting biometric variables in bean during ripening stage. **Idesia**, v. 40, n. 2, p. 39-45, Jun. 2022.

RODRIGUES, G. D. da S.; MOURA, M. S. B. de; SOUZA, L. S. B. de; NASCIMENTO, J. F. do; OLIVEIRA, L. D. da S.; LEO, P. C. de S. Comparação de protocolos de amostragem

para a determinação do índice de área foliar da videira cv. Syrah no Submédio do Vale São Francisco: resultados preliminares. In: JORNADA DE INICIAÇÃO CIENTÍFICA DA EMBRAPA SEMIÁRIDO, 8., 2013, Petrolina. **Anais...** Petrolina: Embrapa Semiárido, 2013. p. 195-201. (Embrapa Semiárido. Documentos, 253).

SANTANA, A. V. de; HEINEMANN, A. B.; STONE, L. F.; NASCENTE, A. S. Índice de refletância na estimativa da área foliar e biomassa das folhas em feijão-comum. **Colloquium Agrariae**, v. 12, n. 1, p. 7-19, jan./jun. 2016.

SILVA, G. D. da; OLIVEIRA, L. D. da S.; VALE, C. N. C. do; SILVA, T. G. F. da; MOURA, M. S. B. de. Calibração do ceptômetro e índice de área foliar da videira em diferentes sistemas de condução no Submédio do Vale do São Francisco. In: JORNADA DE INICIAÇÃO CIENTÍFICA DA EMBRAPA SEMIÁRIDO, 11., 2016, Petrolina. **Anais...** Petrolina: Embrapa Semiárido, 2016. p. 299-304. (Embrapa Semiárido. Documentos, 271).

SOUZA, P. J. de O. P. de; FARIAS, V. D. da S.; LIMA, M. J. A. de; RAMOS, T. F.; SOUSA, A. M. L. de. Cowpea leaf area, biomass production and productivity under different water regimes in Castanhal, Pará, Brazil. **Revista Caatinga**, v. 30, n. 3, p. 748-759, July/Sep. 2017.

STANTON, C.; STAREK, M. J.; ELLIOTT, N.; BREWER, M.; MAEDA, M. M.; CHU, T. Unmanned aircraft system-derived crop height and normalized difference vegetation index metrics for sorghum yield and aphid stress assessment. **Journal of Applied Remote Sensing**, v. 11, n. 2, Article number 026035, June 2017. DOI: 10.1117/1.JRS.11.026035.

THORNTHWAITTE, C. W.; MATHER, J. R. **The water balance**. New Jersey: Drexel institute of technology, 1955. 104 p. (Climatology, v. 8, n. 1).

YU, D.; ZHA, Y.; SHI, L.; JIN, X.; HU, S.; YANG, Q.; HUANG, K.; ZENG, W. Improvement of sugarcane yield estimation by assimilating UAV-derived plant height observations. **European Journal of Agronomy**, v. 121, Article number 126159, Nov. 2020. DOI: 10.1016/j.eja.2020.126159

ZHONG, L.; HU, L.; ZHOU, H. Deep learning based multi-temporal crop classification. **Remote Sensing of Environment**, v. 221, p. 430-443, Feb. 2019.

Embrapa

Meio-Norte



MINISTÉRIO DA
AGRICULTURA
E PECUÁRIA



CGPE 018692